T · H · E
OHIO STATE UNIVERSITY

SEMI ANNUAL PROGRESS REPORT
for the period
June 30, 1988 - December 31, 1988

on

THE EFFECTS OF MAGNETIC NOZZLE CONFIGURATIONS ON PLASMA THRUSTERS

Principal Investigator:

Dr. Thomas M. York
Professor and Chairman
Aeronautical and Astronautical
Engineering Department
The Ohio State University
2036 Neil Avenue Mall, 328 CAE Building
Columbus, Ohio 43210

Technical Officer:

M. A. Mantenieks
Low Thrust Propulsion Branch
MAIL STOP: 500-036
NASA Lewis Research Center
21000 Brookpark Road
Cleveland, Ohio 44135

TABLE OF CONTENTS

TABLE OF CONTENTS, CONT.

ABSTRACT

Plasma thrusters have been operated at power levels from 10kW to 0.1MW. When these devices have had magnetic fields applied to them which form a nozzle configuration for the expanding plasma, they have shown marked increases in exhaust velocity which is in direct proportion to the magnitude of the applied field. Further, recent results have shown that electrode erosion may be influenced by applied magnetic fields. This research effort is directed to the experimental and computational study of the effects of applied magnetic field nozzles in the acceleration of plasma flows. Plasma source devices which eliminate the plasma interaction in normal thrusters are studied as most basic. Normal thruster configurations will be studied without applied fields and with applied magnetic nozzle fields. Unique computational studies will utilize existing codes which accurately include transport processes. Unique diagnostic studies will support the experimental studies to generate new data. Both computation and diagnostics will be combined to indicate the physical mechanisms and transport properties that are operative in order to allow scaling and accurate prediction of thruster performance

I. INTRODUCTION

This research effort was initiated on December 5, 1987, with the specific intent to carry out experimental and theoretical studies of plasma flows within magnetic fields generated by space thruster configurations. The intent was to utilize, and capitalize upon, previous experimental studies and theoretical investigations in order to make rapid progress toward new thruster studies; that indeed has occurred within the reporting period.

A brief outline of the specific study efforts that have been actively pursued were originally presented in the renewal proposal; they are now repeated here to provide a more general description of the progress made.

1. Theory

1.1 Reactivate Numerical Codes for Magnetic Nozzle Effects

Elaborate computational models had been developed to describe the dynamic behavior of plasma within confined magnetic fields. On funding supplied by this grant, a research effort was begun in Summer, 1988, by Mr. P. Mikellides, an M.S. candidate. At this point in time, the whole catalog of computer programs has been installed in The Ohio State University computer system, and can be called up to serve new applications. Some codes have been broken into component parts, and these parts are being used to begin the new studies. However, the first step that had been indicated in the proposal was carried out: a number of relevant codes were successfully re-run to reconfirm previous results.

1.2 Study of Flow Behavior In Magnetic Nozzles with Advanced Physics

The computational models of plasma-magnetic field interaction that were investigated utilized physical principles which could be expected to be consistent and correct. Unfortunately, most simple, classical models of interaction do not, in general, correctly predict plasma behavior, where anomalous transport is almost always evident. Studies have been initiated to test predicted code results against experimental data. Specifically, with experimental results that had been gathered in an earlier experiment, and not properly analyzed, new studies with a 1-D code have already provided new insights. Previous work had used a 0-D code which did not allow local predictions to compare with the location data from experiments. As had been expected, the comparison indicated some

aspects of disagreement using theory based upon classical transport models. In general, this result is a first clue that the anticipated experimental diagnostic studies and detailed studies of alternative models of transport and confinement will be necessary in order to develop a good predictive model of thruster behavior.

2. Experiment

2.1 Develop Experimental Test Facility for Thruster and Magnetic Nozzle Study

Again, there was the intent to utilize much of the existing array of laboratory components for this new application. However, one part of the needed capability was lacking: large vacuum pumps and a large vacuum vessel. Conceptually this has been resolved by the design of an absorption scheme in a small, immovable vacuum tank. The intent is to operate with gas or ablative feed for less than 500 μs, so that saturation of the adsorbers is not complete with the subsequent increase of background pressure. A unique concept that has been applied is the ablative gas sources; the exhaust products will be deposited only when the arc is ignited.

Three different electrode configurations have been fabricated: (1) a large diameter cathode (coaxial) device with ambient gas fill; (2) an enclosed discharge ablative source of magnetic nozzle studies; and (3) a 1/4 scale version of "benchmark" MPD thruster geometry. The coaxial device has been fired successfully many times to test the switch and bench capability.

The magnetic nozzle currently has been designed, fabricated and tested for electrical discharge performance. Further work will continue on the schedule set in the original proposal.

2.2 Conduct Initial Tests With Diagnostics In The Exhaust

Several diagnostic devices had previously been designed, fabricated and utilized in similar studies. These include local pressure probes, local magnetic probes, local Langmuir probes to name a few. Most importantly, Thomson scattering diagnostics for local N_e and T_e measurements had been developed. All these diagnostics are currently available for application to the experiment, on schedule, in the near future.

3. __New Initiatives__

3.1 1/4 Scale MPD Thruster Studies

One of the complementary efforts that had been undertaken during the reporting period was the development of a scaled MPD device that could be studied in detail with the diagnostics being developed. This is important for several reasons, but in particular, with increasingly evident limitations on power in space, a device which could operate on 10-30KW would be attractive to mission planners. This work was carried out by C. Zakrzwski, who returned from a nine-month effort at the Air Force Astronautics Laboratory, Edwards AFB, CA where he worked in the Electrical Propulsion Laboratory. The PI served as his research advisor while he worked at AFAL. Problems with the bank engineering there eliminated the possibility of realistic data taking, but the facilities did allow design, fabrication, and testing to proceed.

3.2 New Diagnostic Studies (Air Force Supported)

The problem of understanding the mechanisms active in plasma thrusters transfers to the problem of developing new and better measurements of plasma properties during the acceleration process. A significant step forward has been taken with the award of a DOD equipment grant to acquire a CW and pulsed CO_1 laser systems which can be used for:

(1) Multi-beam IR and FIR interferometry for Ne

(2) Faraday rotation measurements which indicate B

(3) Measurements of electron density fluctuations.

These new techniques will require considerable effort and time to develop, but will provide a significant improvement in the type of information needed to understand plasma thruster processes.

II. COMPUTER SIMULATION OF PLASMA CONFINEMENT AND FLOW IN A MAGNETIC NOZZLE SYSTEM
(Mikellides)

1. Introduction

The behavior of plasmas in magnetic nozzle geometries being fed by plasma thrusters presents a very complex electromagnetic configuration. One way of understanding this total problem is to examine simpler component problems which will provide insight into component mechanisms which are operative. This section will describe one such effort. Flow from the ends of a theta-pinch is transient, but does provide a good experimental base upon which to construct computational models of plasma behavior. There are no flowing anode-cathode currents and related fields, but nozzle effects are dominant. This work will attempt to apply a code with good geometrical characteristics and full transport description to an experiment which had been very carefully diagnosed. This will result in predictions of transport properties; the code can be extended to include thruster currents, fields, and interactions.

2. Abstract

Experimental results from a 50 cm long linear theta pinch discharge are presented[1] and compared to predictions from a one-dimensional computer simulation[2]. In the experiment, the plasma was generated with a 40 mT D_2 fill in a 3.8 cm radius discharge tube: 67% Z-preionization was followed by a magnetic compression and heating by fields rising to 23 kG in 4.75 μsec. Axial variations of density, temperature and velocity from midcoil to wall contact have been derived from local diagnostics data. Both particle and energy end-loss were treated self consistently in the one-dimensional (1-D) model. The choice of the relevant spatial coordinate being parallel to the compression coil axis enabled modelling of plasma viscosity and the $(jxB)_z$ body force. Exhaust boundary conditions were examined; specifically, models which approximate the interaction of exhaust plasma with background gas and with the vacuum-vessel walls were developed. A radial density profile was assumed by considering a parabolic distribution of the magnetic field inside the plasma column, while temperature was assumed independent of the radius. Number densities are shown to be related to classical transport (classical electrical resistivity). Temperature gradients

do not agree with adiabatic expansion in the flow, but instead show agreement with electron thermal conduction three times the classical value[3]. Although simulation results are in excellent agreement with experiment inside the coil, a need for further investigation outside the compression coil where the expanding magnetic nozzle geometry results in complex plasma-field line interactions.

3. Description of experiment and plasma

To create a theta pinch plasma, a large current is discharged through a single turn coil; this produces a strong time varying axial magnetic field. An azimuthal current sheath is produced in the outer periphery of the gas encircled by the coil. This current sheath interacts with the driving magnetic field to produce a radially inward directed $(jxB)_r$ body force which accelerates the sheath toward the longitudinal axis of the discharge chamber, entraining overrun plasma. Upon reaching the axis, plasma kinetic energy is converted to thermal energy. The thermalized plasma is magnetically confined only in the radial direction; consequently the hot plasma can flow along the magnetic field lines into the exhaust vessel, thus resulting in plasma loss and thermal conduction into the cool exhaust region.

The basic parameters that describe the apparatus and discharge behavior of this particular theta pinch experiment are given in Table I. A schematic of the geometry along with the identification of diagnostics used and their placements are shown in Figure 1.

Table I. Basic Experimental Parameters

I. Geometry

   Coil length: 50 cm   Coil I.D.: 10.5 cm   Tube I.D.: 7.65 cm

II. Fill Gas: Deuterium at 40 mT

III. Plasma Parameters in coil: Peak temperature (T_e-T_i) - 37.4 eV
Peak electron density on axis -
5.02×10^{16} cm^{-3}
Preionization fraction - 67%
Implosion time - 0.80 μsec
Peak driving magnetic field -
23.2 kG
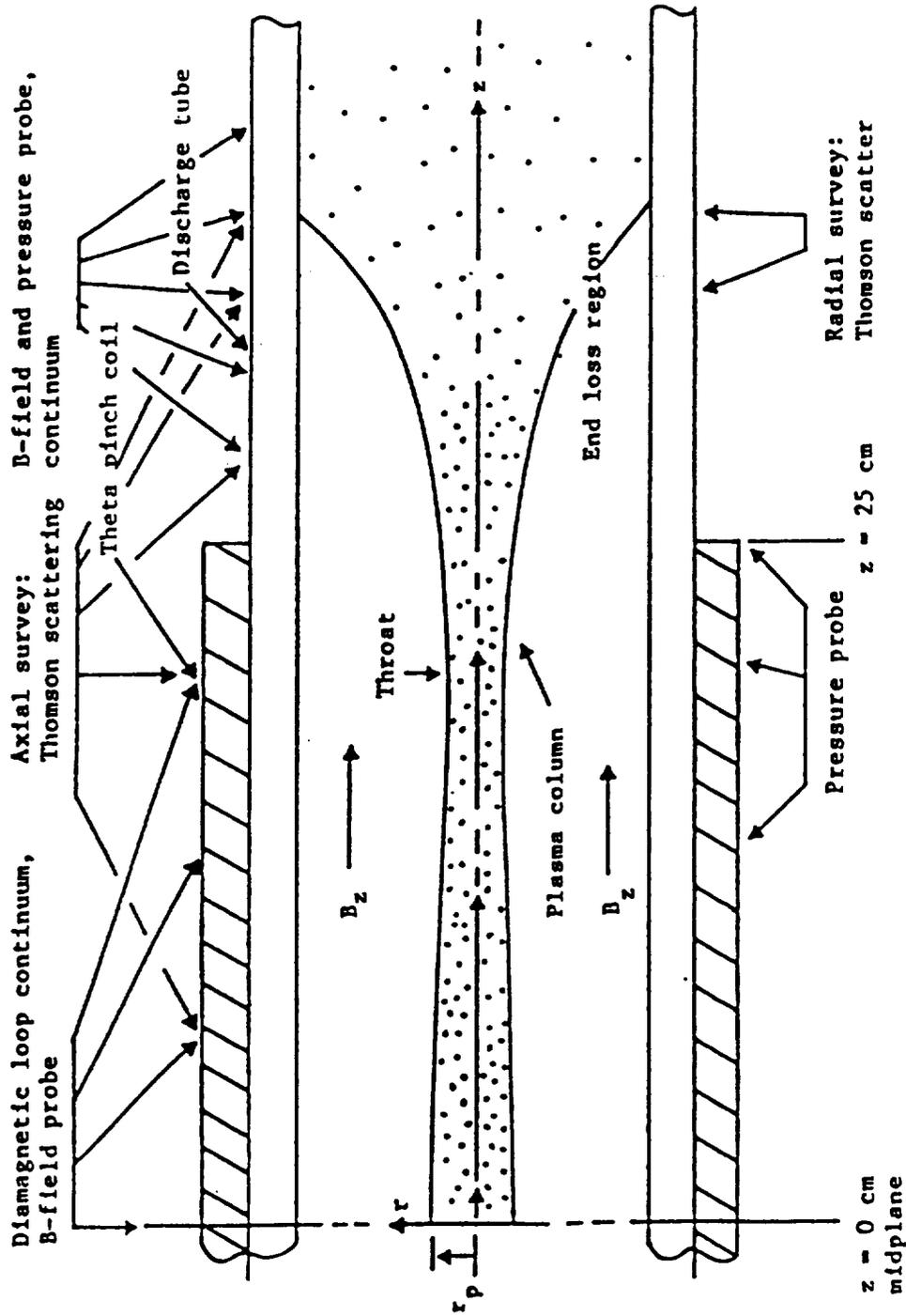
Figure 1. Side view of theta pinch with diagnostic placement.

Values for the axial variation of electron density at different times during the history of the event were taken on center line with a Thomson scattering diagnostic. A combination of data taken with an impact pressure transducer and Thomson scattering made calculations of an experimentally determined axial velocity possible. Thomson scattering diagnostics were also used for the determination of axial variation in electron temperature at different times.

4. One-dimensional plasma model

A time-dependant one-dimensional (1-D) fluid model was used to simulate the open-ended linear theta pinch experiment. The axial coordinate, along the discharge chamber longitudinal axis, was chosen as the relevant spatial coordinate, and the plasma is modelled as a two temperature single fluid which can move with mass averaged velocity directed along the chamber axis. Both ions and electrons are assumed to have nearly isotropic velocity distributions despite the presence of strong magnetic fields; thus each temperature is considered to be independent of direction.

The governing equations adopted for this model consist of five differential equations and a simple mass conservation equation since the choice of a Lagrangian frame of reference which moves with the plasma velocity allows the reduction of the mass conservation equation to a simple algebraic form. The five differential equations include two momentum equations, one each for the radial and axial directions; two temperature equations, one for each species; a magnetic flux equation and a description of the driving vacuum magnetic field. The following physical phenomena were incorporated: work done on the plasma rising from motion of the plasma; electron thermal conduction; electron-ion thermal equilibration; viscosity; electrical resistivity; magnetic field curvature effects; and vacuum-vessel sidewall and end-wall interaction with the exhaust plasma. A diffuse radial profile defined by a parabolic distribution of the magnetic field inside the plasma column was examined.

These equations are differenced either explicitly or implicitly depending upon the importance of diffusion terms such as thermal conduction. When diffusive terms are dominant, they are differenced implicitly because of numerical stability considerations. This requires the inversion of a matrix,

which varies in size from 20x20 to 40x40, at least once per time step. Weakly diffusive terms are explicitly differenced when possible thereby easing computational costs. All other terms are, in general, differenced explicitly.

Appropriate boundary and initial conditions were included to complete the fluid plasma description.

5. One-dimensional simulation

Simulation of the plasma behavior started at the end of the dynamic implosion which occurred at 0.8 μsec. The following experimental values were used to begin computational simulation:

Implosion velocity:	7.17 + 0.43 cm/μsec
Implosion time:	0.800 + 0.30 μsec
Electron temperature:	20.7 + 3.3 eV
Plasma radius:	1.97 + 0.38 cm
Electron density:	4.34 + 0.61 x 10^{15} cm^{-3}

In addition, an experimentally determined beta ($\beta = nkT/(B^2/8\pi)$) on-axis of 0.94 at 0.85 μsec was used. Number density, n(r) is a function of radius. Thus an average ratio, of the on axis magnetic field, B_a, to the driving magnetic field, B_e, was determined from the parabolic distribution of the field inside the plasma column, $B_i(r)$,

$$B_i(r) = B_a + (B_e - B_a) \; r^2/a^2, \; r \leq a$$
$$B_i(r) = B_e, \qquad\qquad r > a$$

where a is the radius of the plasma column. The above expression can be written in the following manner in order to normalize over the plasma radius:

$$\delta_i(r) = \delta_a + (1-\delta_a) \; r^2/a^2, \; r \leq a \; \text{and} \; \delta_i(r) = 1, \; r > a$$

where $\delta_i(r) = B_i(r)/B_e$ and $\delta_a = B_a/B_e$.

Consequently, a radial average was determined by

$$\bar{\delta} = 1/a \int_0^a [\delta_a + (1-\delta_a) \; r^2/a^2] \; dr = 2\delta_a/3 + 1/3,$$

which was used in conjunction with a $\beta_a - 1 - \delta_a^2$ of 0.9 at implosion to determine an average value for the number density from pressure balance in the radial direction,

$$2\bar{n}kT - \beta \ B_a^2/8\pi$$

with $\beta - 1 - (\bar{\delta})^2$.

Thus, with the above considerations the following implosion values were chosen to begin simulation, within experimental error for best agreement:

Implosion time: 0.8 μsec
Electron temperature: 18 eV
Plasma cross sectional area: 8.0 cm^2
Electron number density: 1.78 x 10^{16} cm^{-3}

Implosion values were assumed uniform along the axial coordinate, z. At 0.8 μsec the driving magnetic field strength was 6.07 kG which results in an initial flux value of 31.96 Maxwells. At this time only background compression effects of the cold gas, taken at fill density of 2.63 x 10^{15} cm^{-3} and 0 eV, were included. Sidewall interactions, magnetic field curvature effects and pseudoviscous effects were excluded.

5.1. Midplane and axial behavior of electron number density

Midplane electron number density variation with respect to time is shown in Figure 2. Good agreement was achieved by using finite plasma electrical resistivity to current flow across the strong magnetic field, η_1. This value was taken to be that of the classical expression[4],

$$\eta_{CL} - 3.67 \ x \ 10^{-19} \ n\lambda/T_e^{3/2}$$

where $n\lambda$ is the coulombic logarithm. This result is quite important yet not surprising since the diffusion of applied magnetic field into the plasma column must result in a diffusion of plasma particles to larger radii if radial pressure balance is to be satisfied. Satisfaction of mass conservation requires that number density must then decrease. In addition, the use of finite resistivity supports the choice of a diffuse parabolic profile for the magnetic field inside the plasma column instead of a uniform profile which would have forced a constant value of flux inside the column and thus, in general, higher number density.
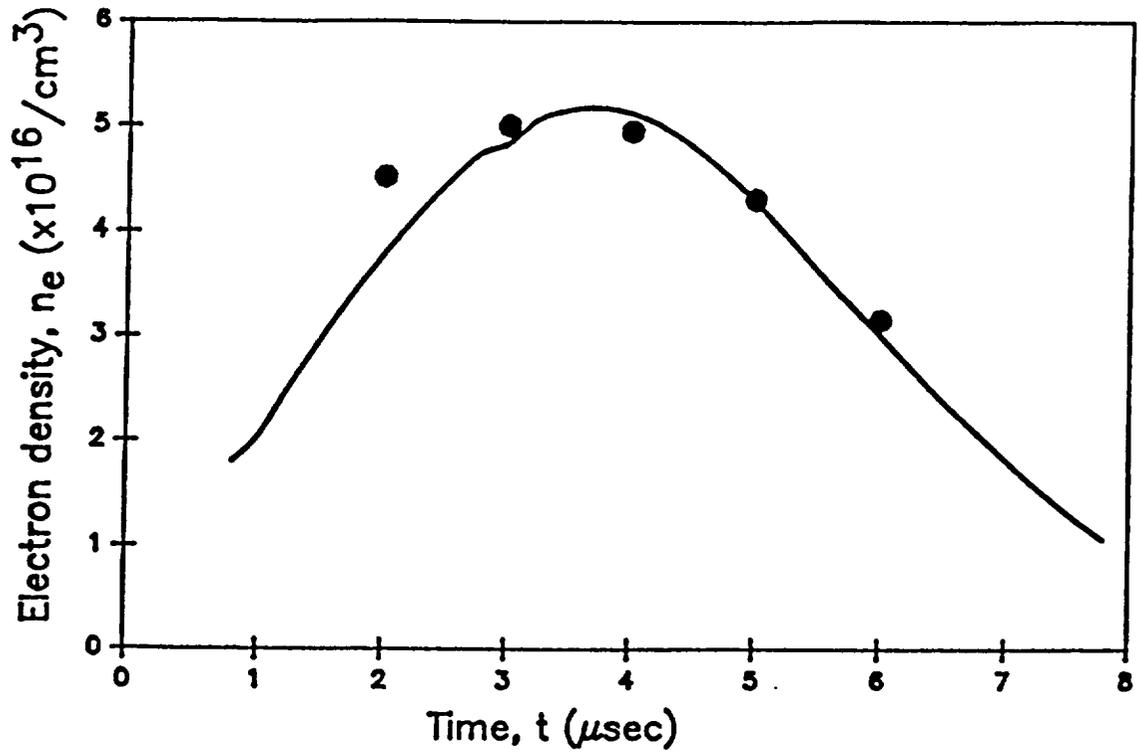
Figure 2. Midplane electron number density profile
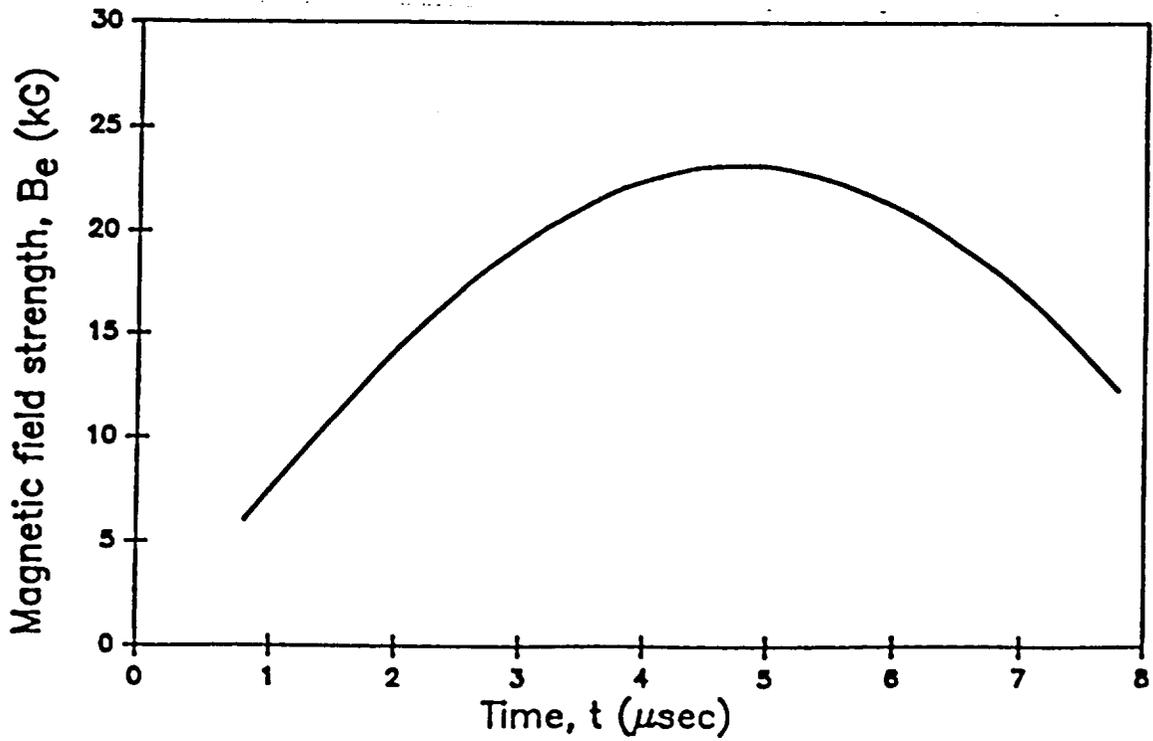
Figure 3. Applied magnetic field strength

Good agreement with experimental results is also evident in the axial variation of the number density both inside and outside the compression coil. These profiles are shown in Figures 4,5,6 and 7.

However, at two instants, 3 and 4 μsec simulation results are lower than the experimental number density values at a location 20 cm from midplane. This could be the result of an expansion wave travelling upstream; it would be formed by pressure imbalance between the background gas pressure and the plasma pressure inside the coil. Excellent agreement at later times supports the notion that such a wave has reached the midplane location, and it is no longer influential. Pseudoviscous effects will be investigated with a concern for different treatment of shock regions. Another possibility is that anomalous plasma resistivity resulting from lower hybrid drift microinstabilities can no longer be considered to be negligible in these regions.

5.2. Midplane and axial behavior of electron temperature

Midplane and axial electron temperature profiles are shown in Figures 8, 10, 11, 12 and 13. Again very good agreement is evident between experimental and simulation values.

The 1-D model included both thermal conduction parallel to the discharge axis as well as heat conduction from the plasma across the magnetic field lines. Thermal conduction parallel to the axial coordinate was represented by[2]

$$q_e - -K_e 2T_e/2z,$$

where $K_e - 6.119 \times 10^{28} \, T_e^{5/2}/ \, n\lambda$ (1/cm-sec) and q_e was the electron heat flux directed along the guiding magnetic field. Heat flux from the plasma across the magnetic field lines into the exhaust-vessel sidewalls was represented by K_e[3]. Adiabatic expressions for the plasma expansion flow resulted in electron temperatures about 1.5 times higher than the experimental results. This disagreement indicated use of the classical collisional expression for electron thermal heat flux. The satisfactory agreement in both midplane and axial variations was achieved by increasing this classical expression by a factor of 3. This result shows that the flow is not adiabatic, but rather that heat losses are quite substantial.
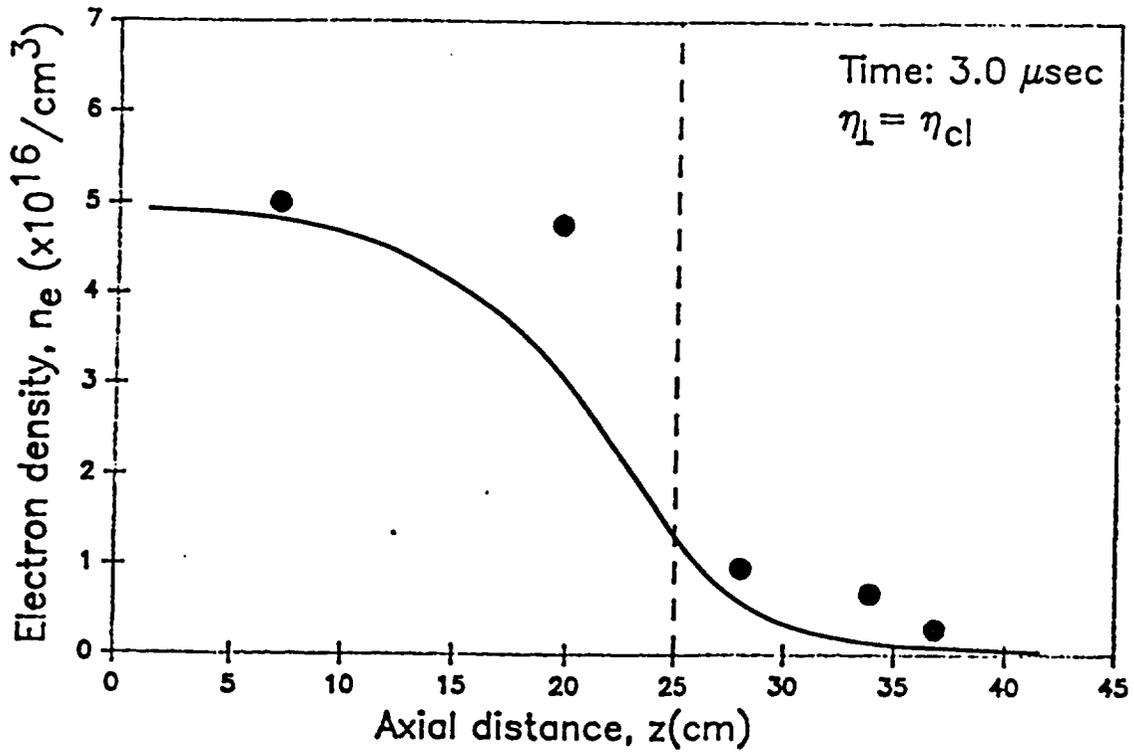
Figure 4. Axial variation of number density at time, t= 3.0 μsec
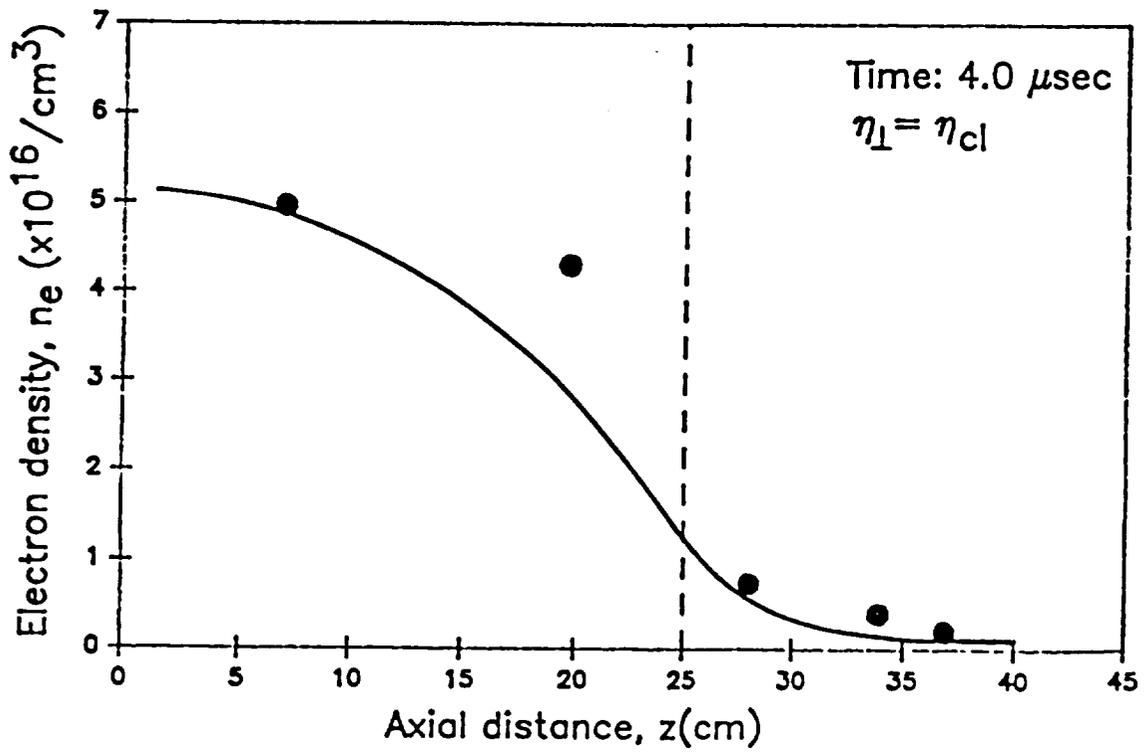
Figure 5. Axial variation of number density at time, t= 4.0 μsec
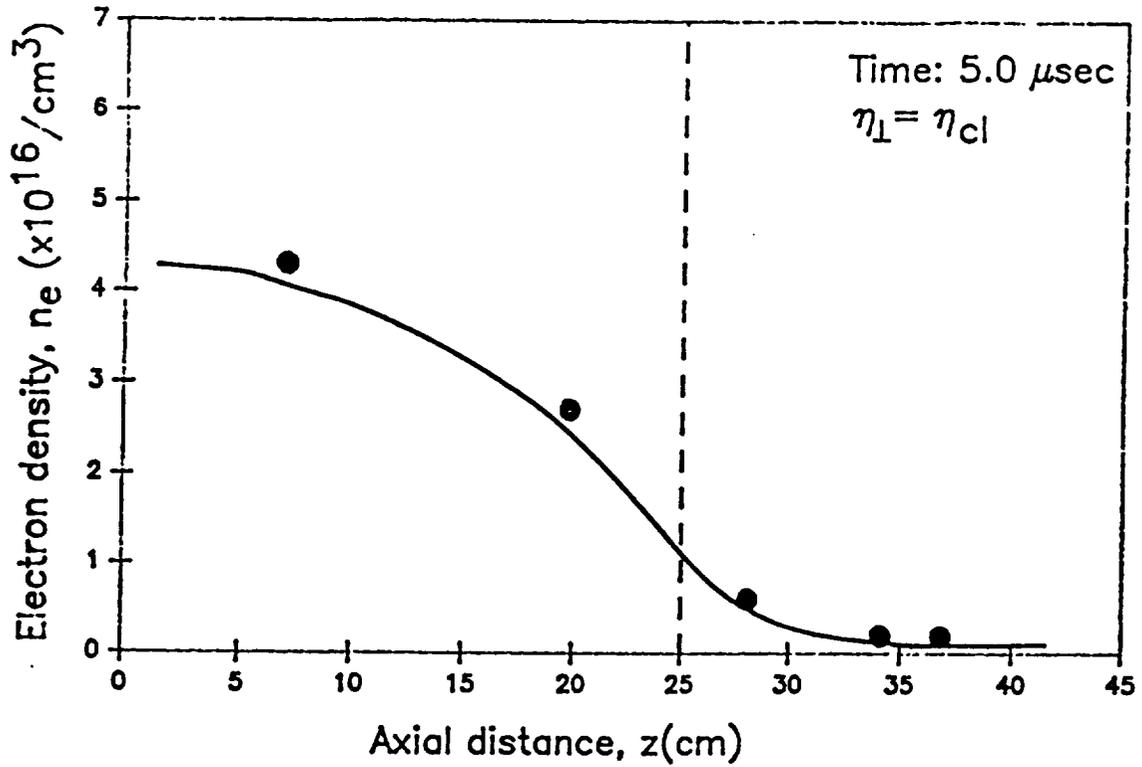
Figure 6. Axial variation of number density at time, t= 5.0 μsec
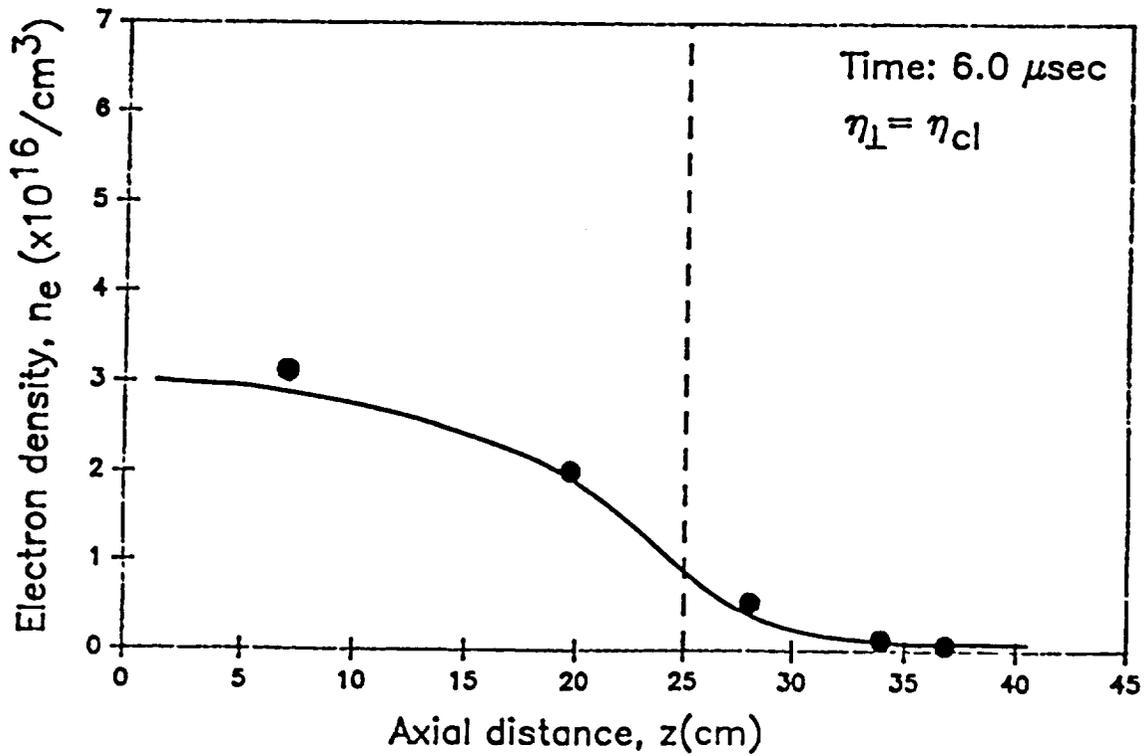
Figure 7. Axial variation of number density at time, t= 6.0 μsec
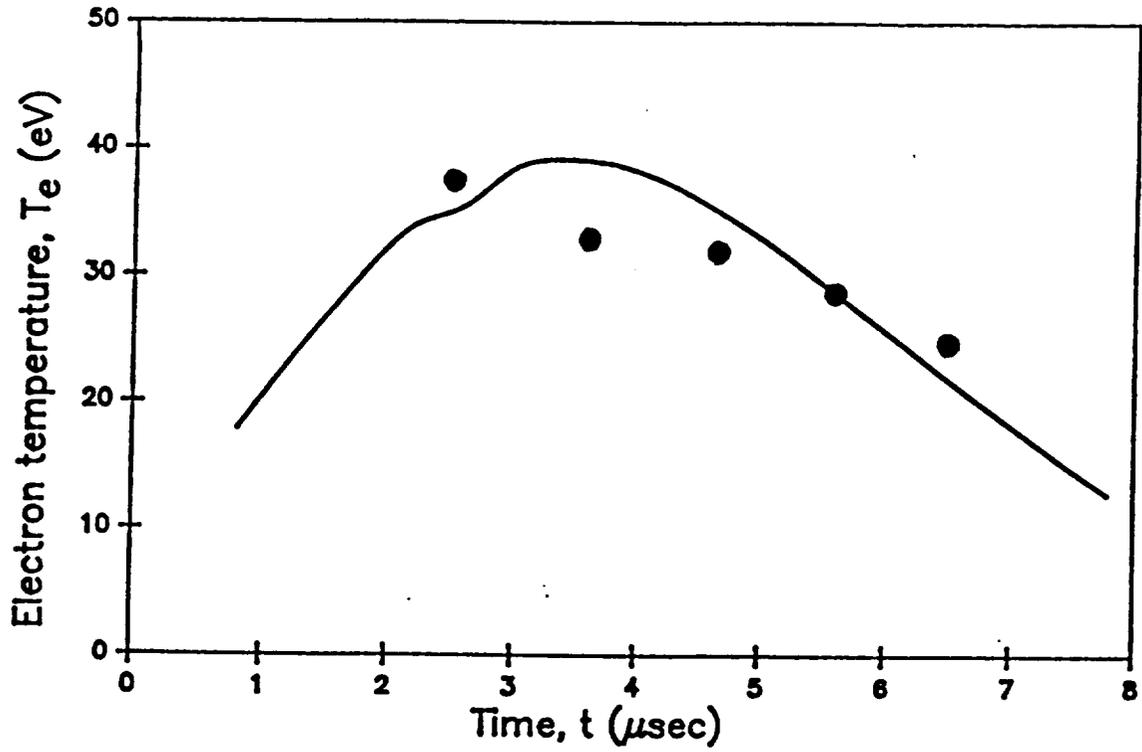
Figure 8. Midplane electron temperature profile
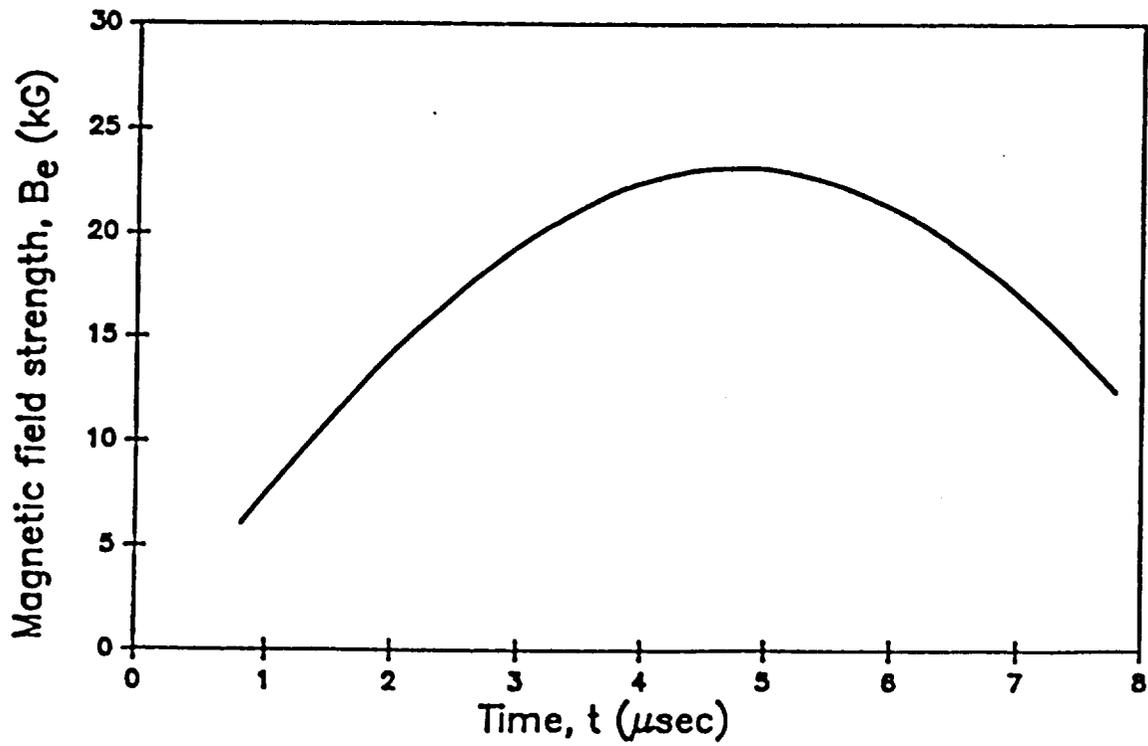
Figure 9. Applied magnetic field strength
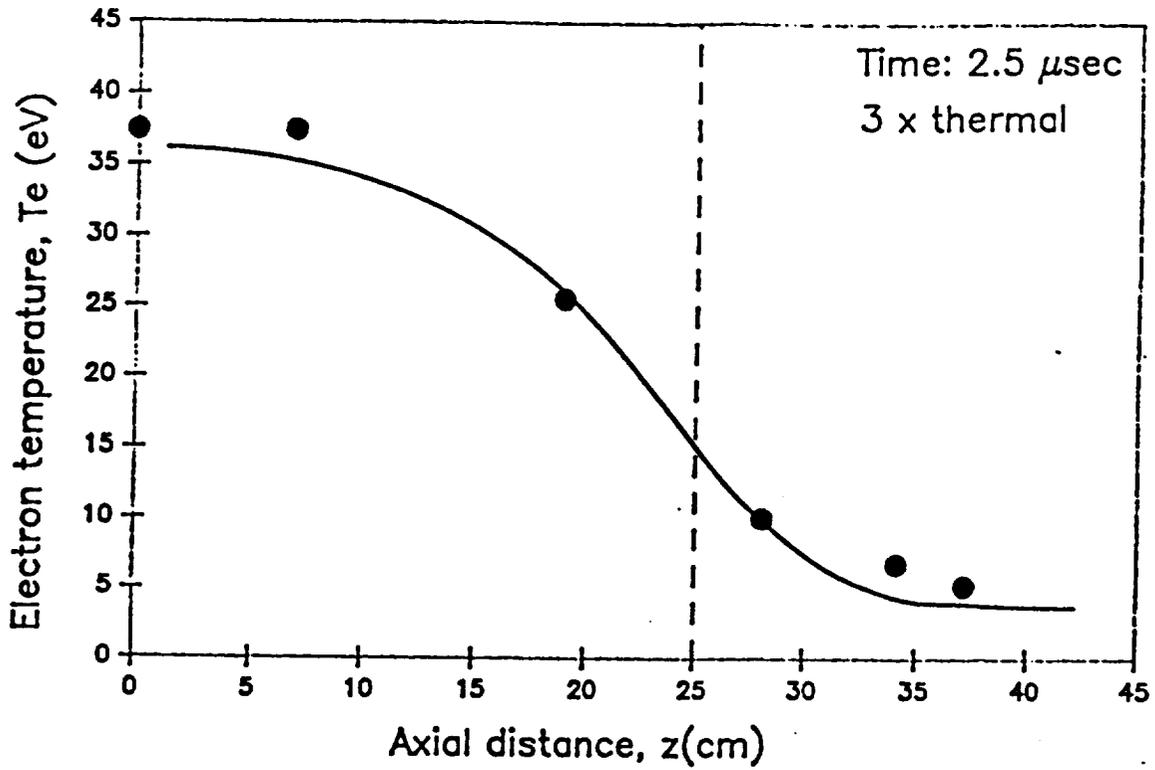
Figure 10. Axial variation of electron temperature at t= 2.5 μsec
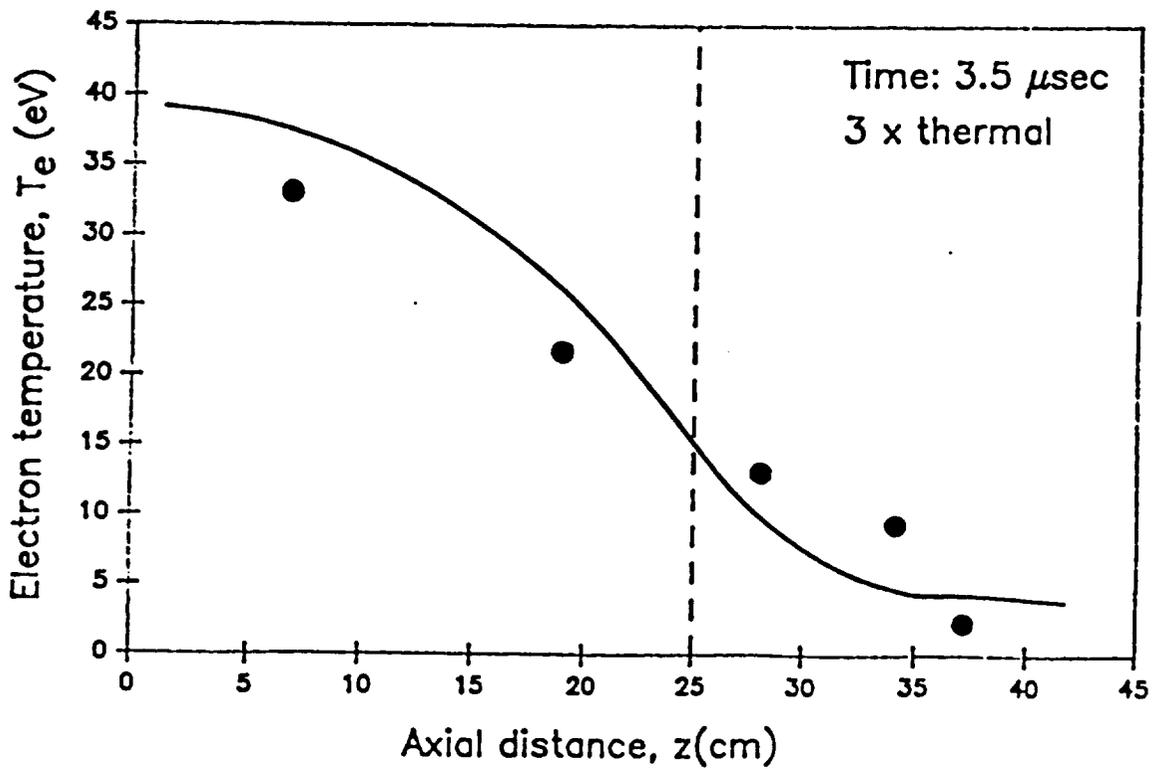
Figure 11. Axial variation of electron temperature at t= 3.5 μsec
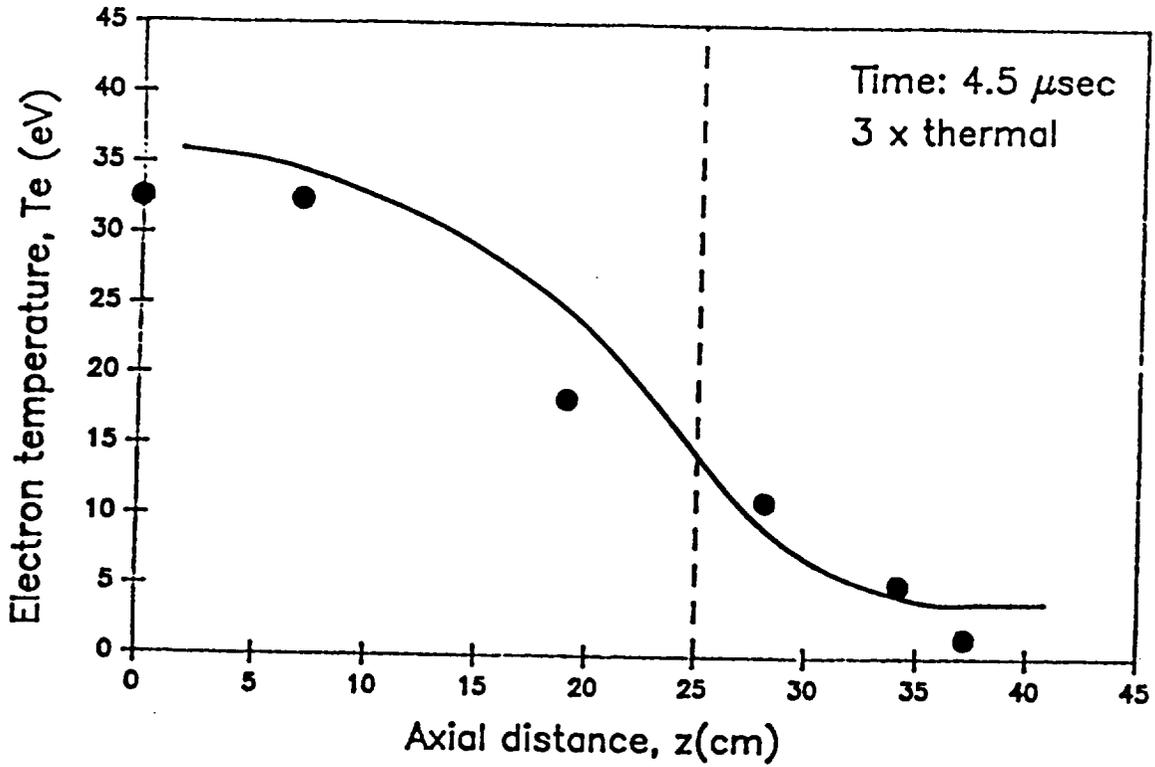
Figure 12. Axial variation of electron temperature at t= 4.5 μsec
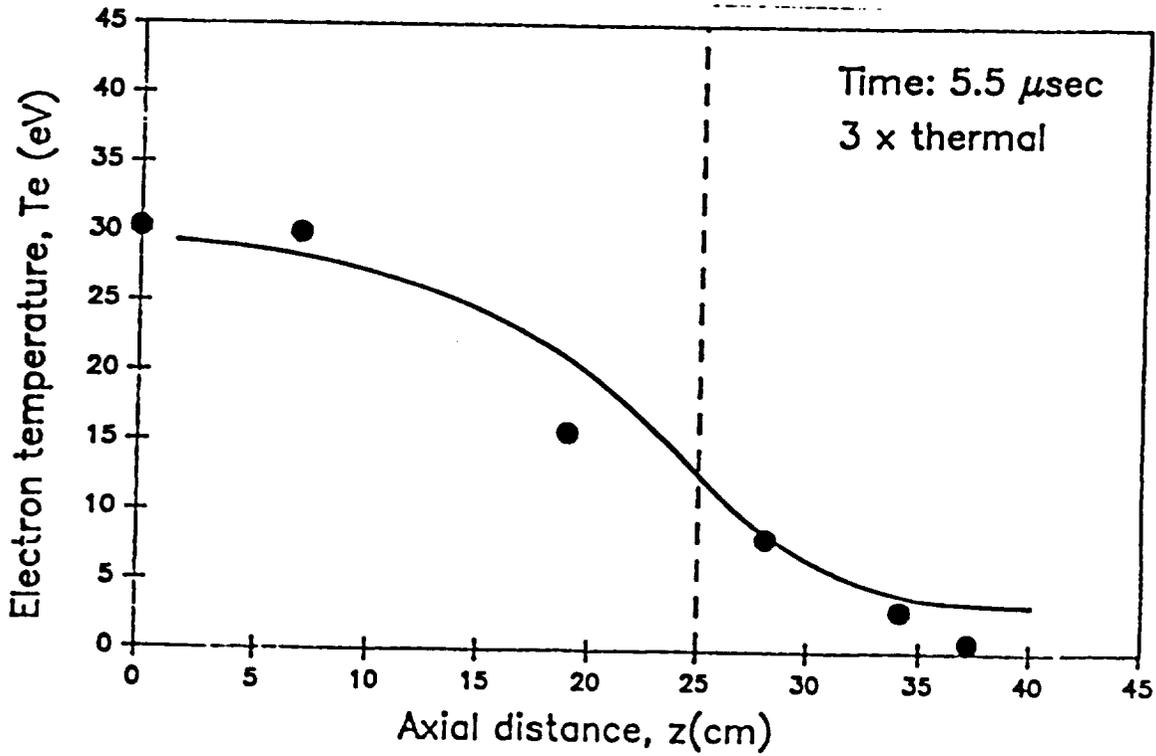
Figure 13. Axial variation of electron temperature at t= 5.5 μsec

5.3. Axial behavior of plasma cross sectional area inside and outside the compression coil

Figures 14, 15, 16, and 17 show the axial variation of the plasma cross sectional area inside the compression coil at different times during the history of the event. Experimental results, again show substantial agreement with the theoretical ones; they show formation of a throat, that is, a decrease in the cross sectional area in the vicinity of 18.5 cm from the midplane. This formation results from a decrease in thermal pressure due to the conversion of thermal energy into directed kinetic energy along the axial coordinate. Simulated values show the throat to be formed at about the same location, but it was not as evident. This could be a result of an incorrect simulation of background gas compression effects in conjunction with the magnetic field pressure outside the confined plasma.

A need for further investigation of these effects is evident in Figure 18 in which experimental values of plasma radius outside the compression coil are compared to the simulated ones. It has been determined that choice of a lower density for cold gas results in better agreement. This shows that the simulated thermal pressure inside the plasma column expanding to the exhaust-vessel sidewalls is higher than the one needed to balance the applied magnetic field pressure which rapidly decreases outside the coil.

Inclusion of sidewall influence on the expanded plasma as it hits the vessel boundaries improves the comparison by constraining the plasma velocity and heat transfer to the walls to zero.

5.4. Axial behavior of plasma velocity inside and outside the compression coil

Comparisons of plasma velocity variation (Figures 19 and 20) through the nozzle show general agreement between experiment and theory. Both experimental and simulated results show the gradual conversion of thermal energy into directed kinetic energy along the discharge axis, reaching sonic velocities at the throat.

However, at 3.0 μsec a rapid decrease in velocity outside the coil shown by the experiment confirms a need for a further examination of background gas effects and applied magnetic pressure effects. In the simulation, increasing number density for the cold gas shows an improved comparison, but this effect opposes the tendency for better agreement in the plasma radius comparisons. It
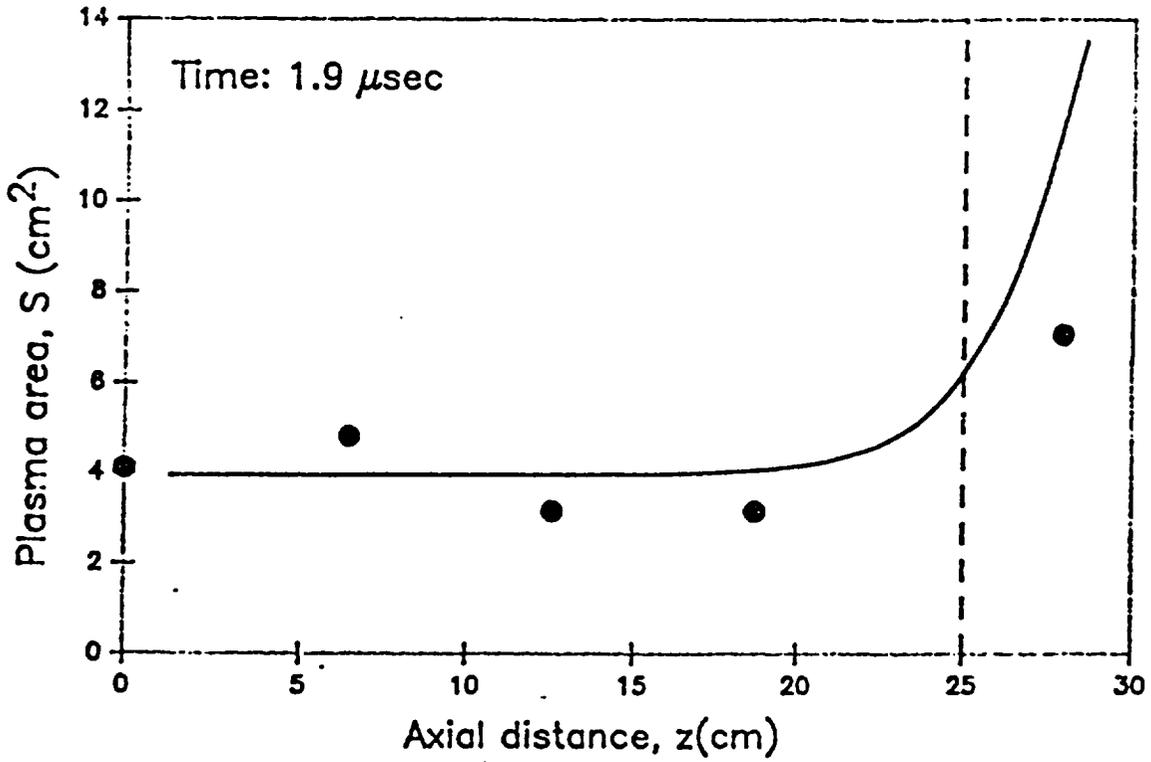
Figure 14. Axial variation of plasma cross sectional area at t= 1.9
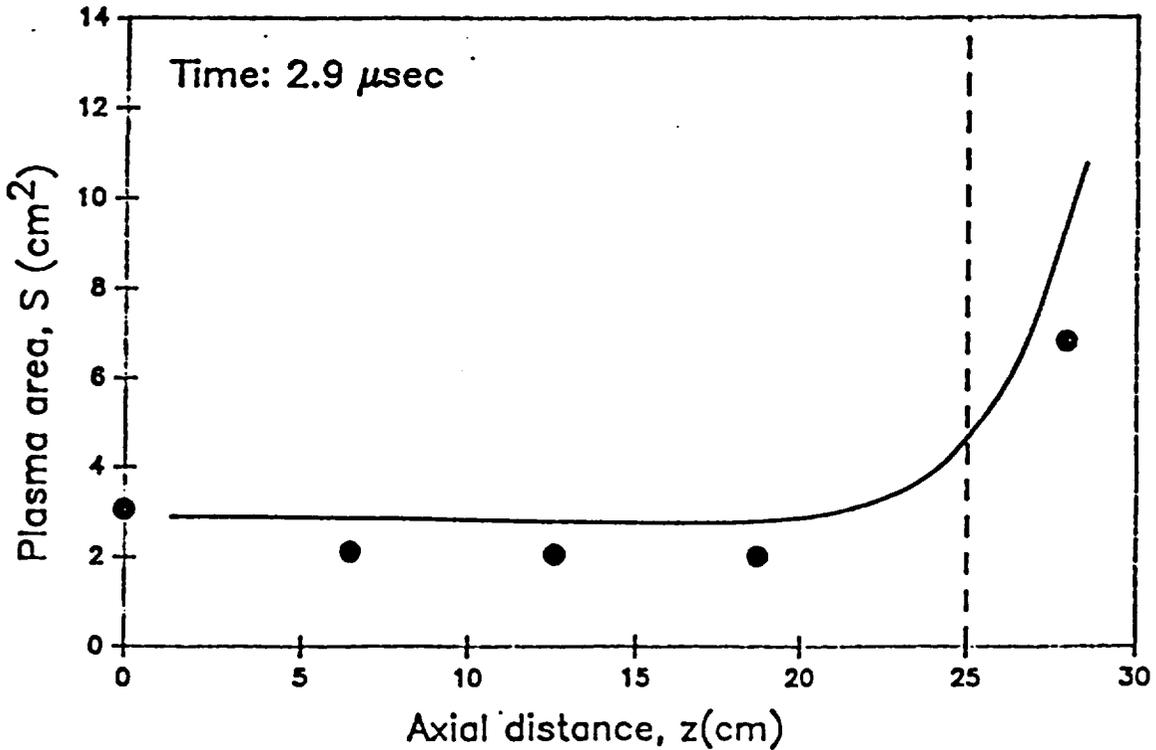
Figure 15. Axial variation of plasma cross sectional area at t= 2.9
μsec
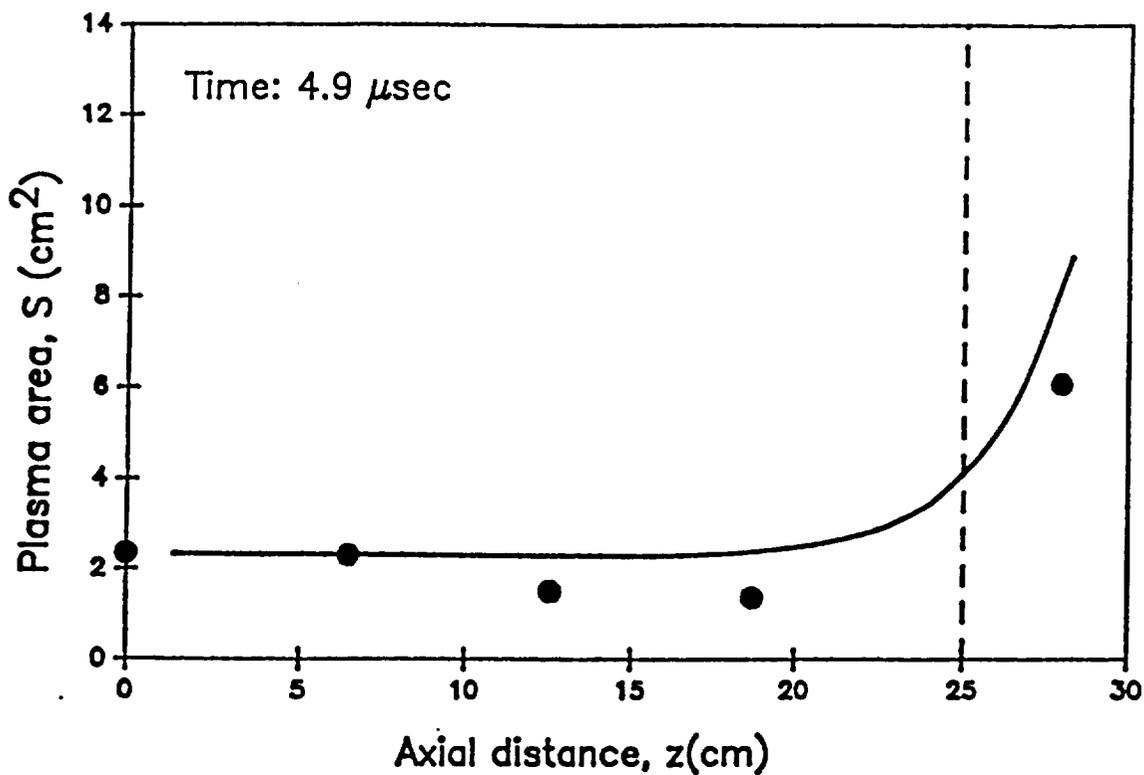
Figure 16. Axial variation of plasma cross sectional area at t= 4.9 μsec
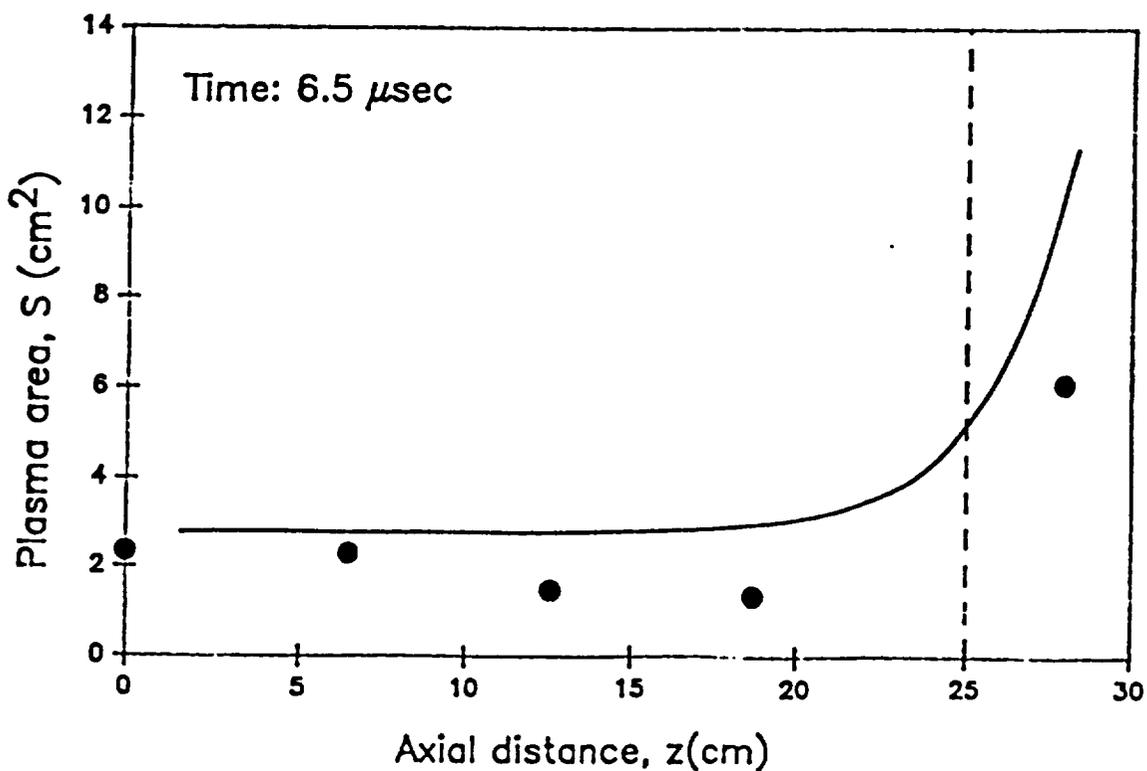
Figure 17. Axial variation of plasma cross sectional area at t= 6.5 μsec
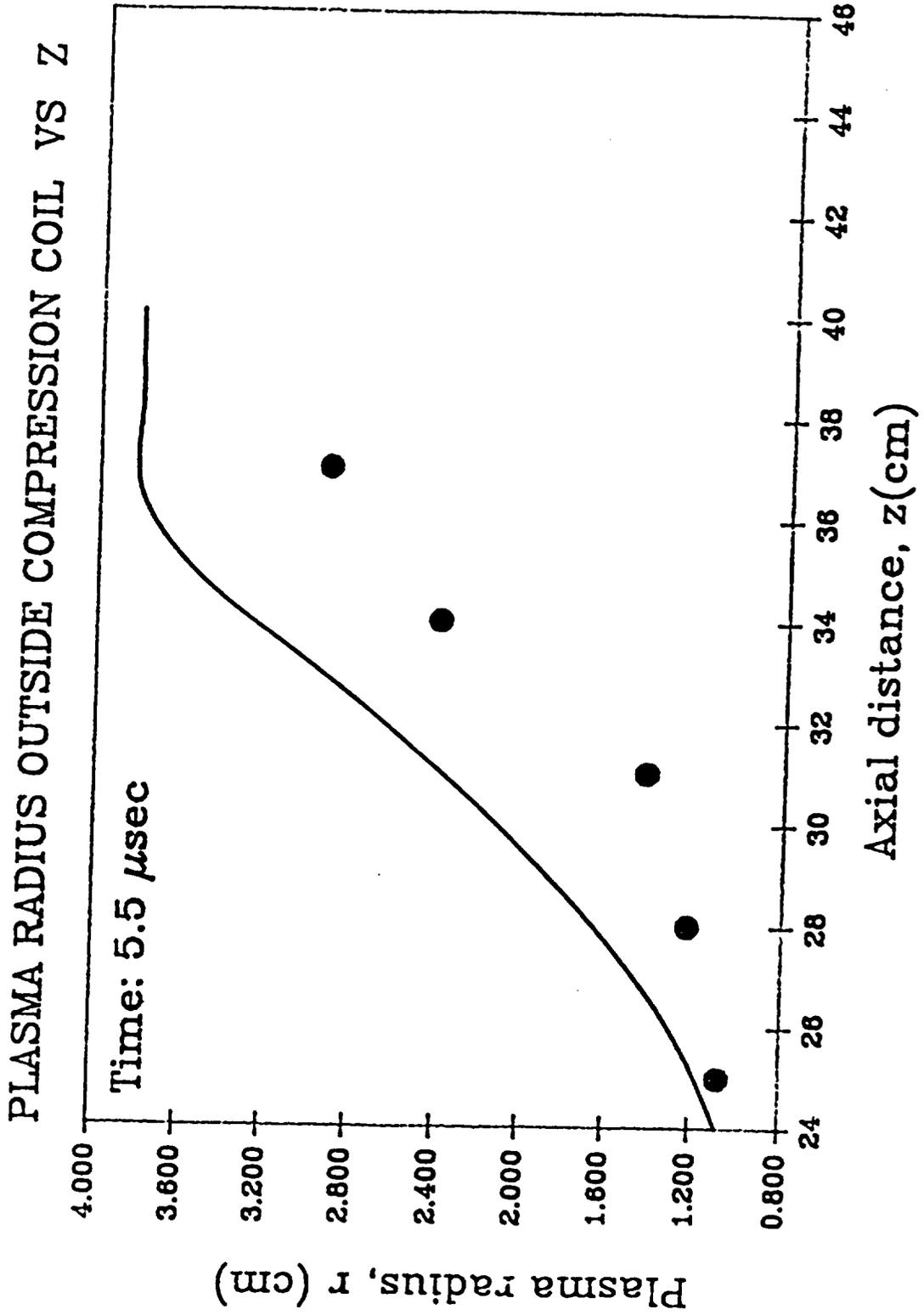
Figure 18. Axial variation of plasma radius outside the compression coil at time, t= 5.5 μsec
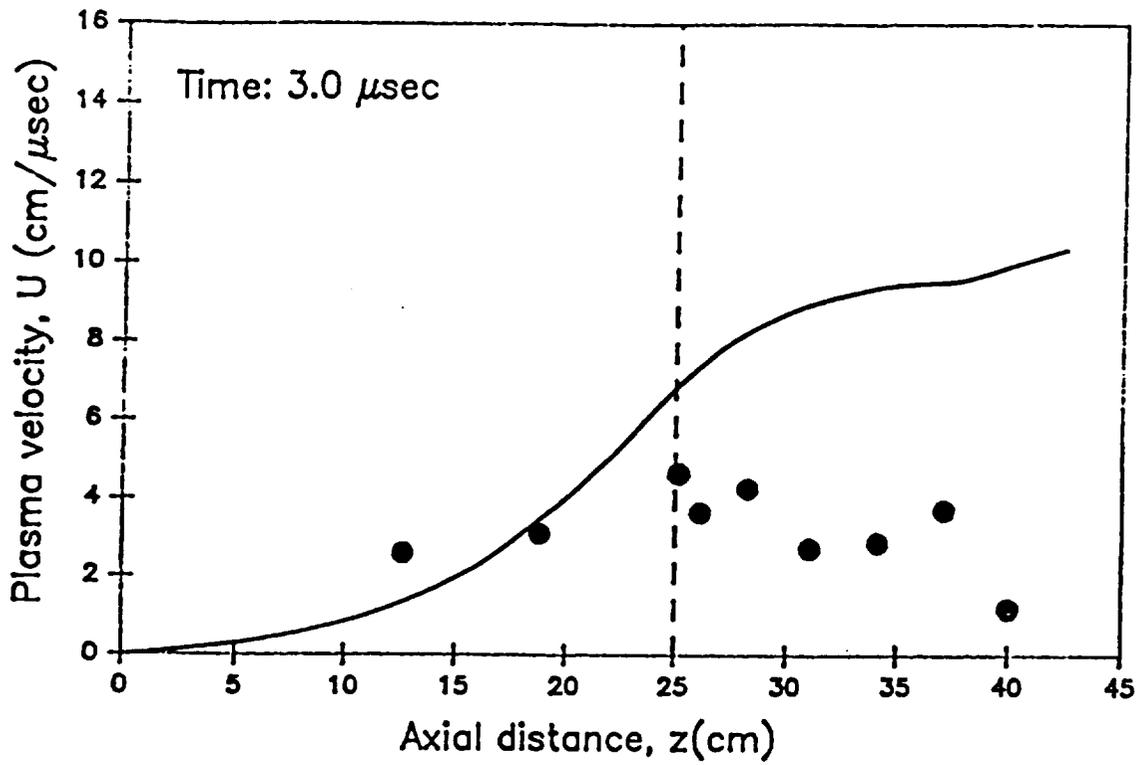
Figure 19. Axial variation of plasma velocity at t= 3.0 μsec
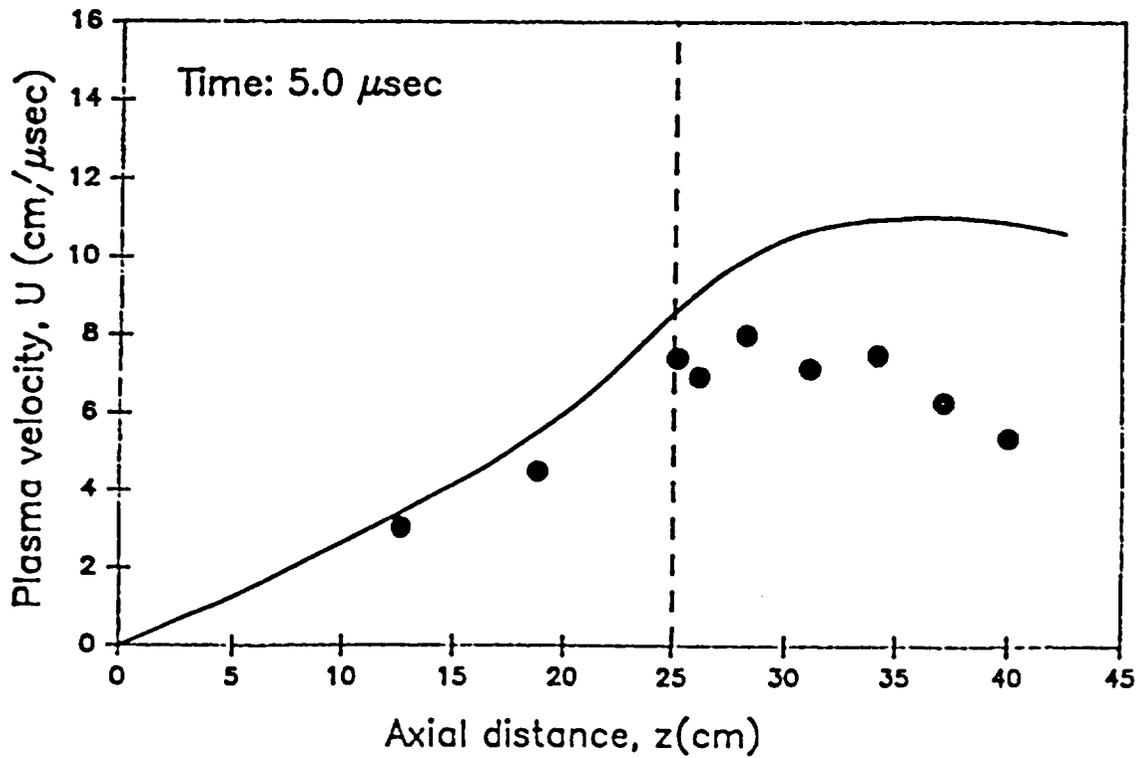
Figure 20. Axial variation of plasma velocity at t= 5.0 μsec

is possible that at a constraint of zero velocity on the sidewalls instead of free expansion will significantly improve the results.

6. Summary and Conclusions

A study of plasma transport in open-ended theta pinches has been presented by comparing results from a cold, collisional 50 cm theta pinch experiment and a one-dimensional plasma simulation model. Agreement between these results required that expansion inside the compression coil is not compatible with an adiabatic profile, but instead, that heat conduction is quite evident. Best agreement was achieved when a classical resistivity expression was used to simulate plasma electrical conductivity across magnetic field lines and thermal conductivity was taken to 3x classical.

A throat was seen to form at 18.5 cm from the midplane, indicating a minimum in thermal pressure, and the velocities at the throat approached sonic speeds.

Further investigation is required for a better description of plasma processes outside the compression coil. A combination of sidewall influences and applied magnetic field pressure effects are believed to be a part of an improved solution.

III. EXPERIMENTAL APPARATUS FOR MAGNETIC NOZZLE AND THRUSTER STUDIES
(Soulas and Zakrzwski)

1. Introduction

The apparatus that has been developed for the experimental studies includes a number of component parts. While the end result must be the electrical discharge of a device that generates plasma for studies of flow within a magnetic nozzle or the electrical discharge of a thruster configuration, the supporting system can dictate the over-all system performance. In this case the available vacuum system does constrain the whole experiment, since no large tank or steady state pumping capacity is available, the electrical devices and discharge period must be tailored to meet that constraint. The utilization of relatively small bore (6 inch diameter) pyrex duct to form an exhaust vessel can be supplemented with an absorption scheme to inhibit backstreaming. However, test time will still be limited to 200-400μs. Since gas flow can only be allowed for the time of active discharge, the use of an ablative thruster is most appropriate.

The experimental apparatus will be described in four sections. First, the vacuum system, including all equipment needed for its operation, will be described. Second, the electrical discharge system will be discussed. This includes a description of the design of a pulse-forming network and the unique design of the spark-gap switches. Third, the design of two of the principle thrusters, the ablative and coaxial thrusters, and the magnetic field nozzle will be discussed. Finally, the diagnostic devices used to measure current in electrical discharge system and the magnetic field generated by the magnetic filed nozzle will be noted.

2. Vacuum System

The vacuum system was designed to allow the study of the plasma flow using existing equipment. It consists of a cross-shaped 6-inch inner diameter pyrex duct, a T-shaped, 6-inch inner diameter pyrex duct, a 4-inch electropneumatic gate valve (Parker-Hannifin, Des Plaines, Illinois) and a Duo-Seal Vacuum Pump Model No. 1397B (Welch Vacuum Products, Chicago, Illinois), which can displace 15 cubic feet per minute. Figure 21 illustrates the components.

The vacuum system is divided into two sections separated by the electropneumatic gate valve. The upper section consists of T-shaped and cross-shaped
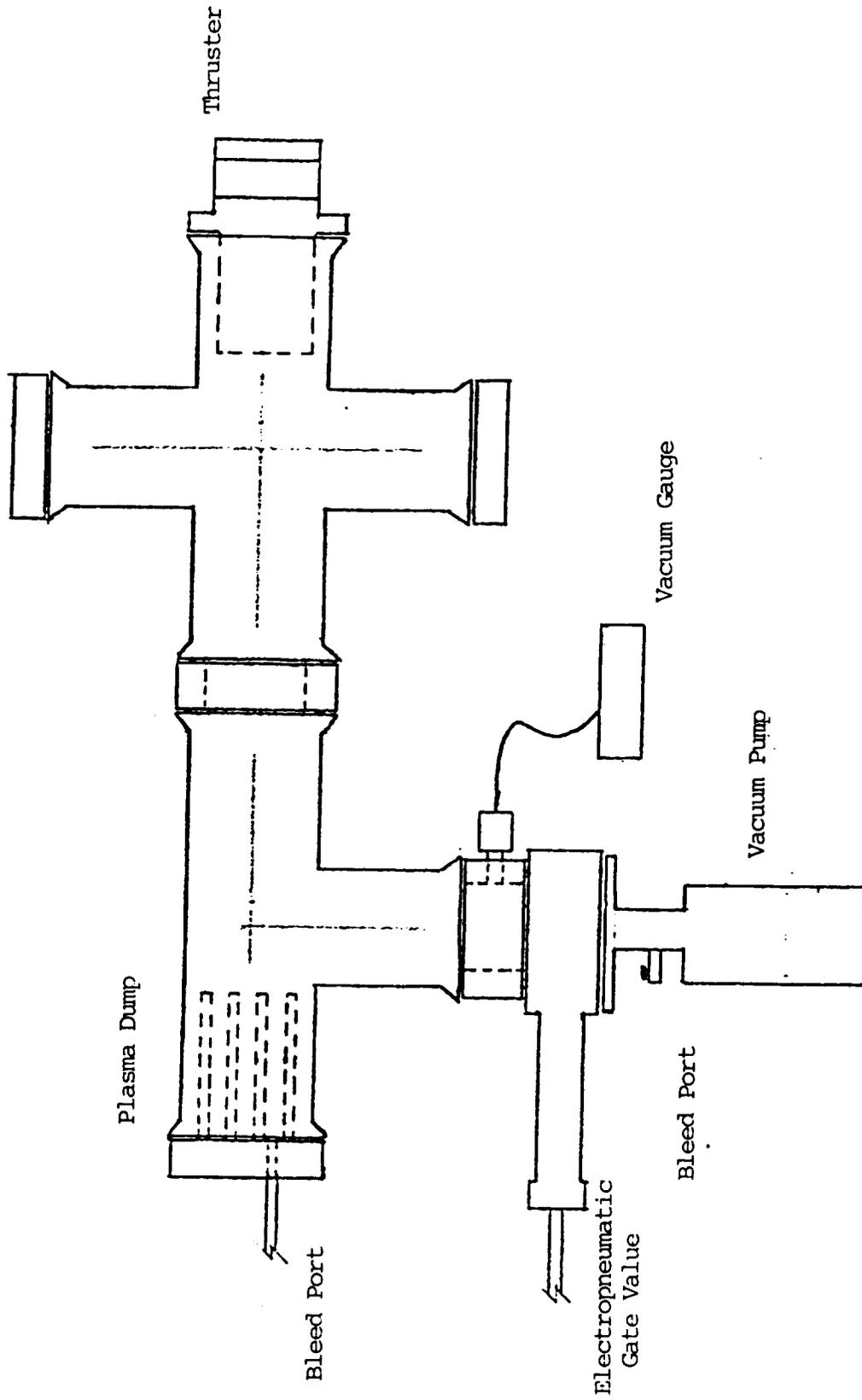
Figure 21. Vacuum System Schematic

ducts interconnected. The cross-shaped duct houses the thruster on one end; this allows diagnosis of the plasma to be carried out through the side arms within the test cavity. The T-shaped tube has a plasma dump, i.e. an arrangement of brass rods which will absorb the plasma ejected from the ablative thrusters, and a port for bleeding in nitrogen fill gas for coaxial thruster experiments. Between this duct and the electropneumatic gate valve, there is a pressure port which accommodates a vacuum gauge, an MKS Thermal Conductivity Vacuum Gauge, Model TC-1 (MKS Vacuum Systems, Burlington, Massachusetts). Currently, a base vacuum pressure of 2 millitorr can be achieved. All open ends of the glass tubes are capped off with machined plexiglass. The lower section consists of the vacuum pump capped by a transition section fitted with a bleed port for venting the pump to the atmosphere.

3. Electrical Discharge System

The main purpose of the electrical discharge system is to produce the quasi-steady currents needed to create the plasma and magnetic fields of the experiment. Specifically, this requires a pulse that ranges from 1-10kA in magnitude with a run time of 200-500μ sec. To produce this quasi-steady current, a pulse forming network utilizing energy discharge capacitors (Maxwell Laboratories, San Diego, California), with a capacitance of 14μ F and a maximum voltage of 20kV, in conjunction with a spark-gap switching scheme has been used.

a) Pulse Forming Net (PFN)

The PFN is the L-C ladder shown in Figure 22. The load represents one of the thrusters or the magnetic field coil. When firing the electrical discharge system, two independent PFNs are discharged simultaneously (one PFN for the thruster and one PFN for the magnetic field nozzle). The output of the bank has been tailored to meet the requirements listed above by varying the individual stage inductances and the load resistance. These values for inductance and resistance have been determined through the use of a computer program which solves the system of equations which describe the electric circuit.

There are currently two basic configurations for each PFN. The first, utilizes only four capacitors, can achieve a run time of 250 μsec. The inductances between each stage are: $L_1 - L_2 - L_3 - L_4 - 100\mu$H.
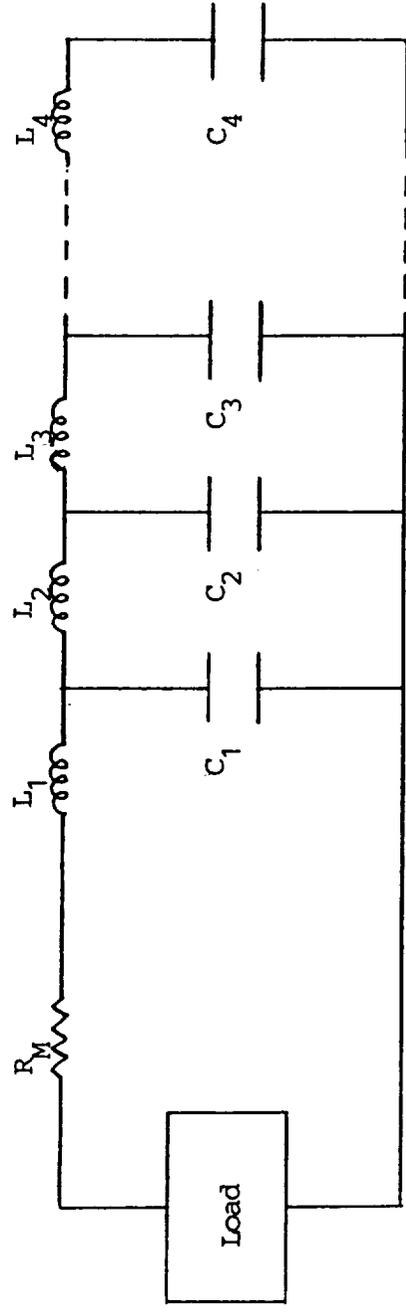
Figure 22. Pulse Forming Network Schematic

The matching load resistance, $R_M = 0.5\Omega$. If the capacitors are initially charged to 12kV, a quasi-steady current of 3.5kAmp can be attained. For 18kV charge, 7kA are attained; for 7.5kV charge, 2.2kA are attained. The numerical solution for the circuit current at 12kV is shown in Figure 23.

Both configurations have sharp rise times, on the order of 50 μsec., and relatively steep fall times. It should be noted that the magnitude of the current is best adjusted by varying the initial voltage of the capacitors, and the length of the current pulse is best increased by adding more stages.

The components fabricated for the PFN included the stage inductors and the load resistor. The stage inductors are made of No. 8, solid core, copper wire with THW insulation (rated at 600V) coiled around an 8.75 inch, outer diameter, schedule 40 PVC pipe, with a 10.75 inch diameter flange. In order to allow the inductors to be used interchangeable between each configuration, 50 μH, 100 μH and 200 μH inductors were made. They can be connected in series so as to create the needed stage inductance. The load resistor is made of two rectangular copper sheets, each with an area of 135 square inches and separated 1 inch by plexiglass blocks, completely immersed in a solution of distilled water and copper sulfate. This design allows the value of the load resistance to be charged by changing the concentration of the solution.

b) Spark Gap Switching Scheme

The PFN is fired by means of two spark gap switches. A circuit diagram of the charging and discharging system is shown in Figure 24.

A high voltage D.C. supply (Del Electronics, Mt. Vernon, New York), with a maximum voltage capability of 30kV, is used to charge the capacitor bank of the PFN to the desired voltage. A capacitor bleed is provided to discharge the bank whenever it is necessary. The capacitor bank energy is discharged to the thrusters or magnetic field nozzle, by means of two interconnected spark-gap switches.

The firing switch triggers an SCR Marx array which generates a high voltage pulse to the center pin of switch #1 which causes an arc between the center pin and surrounding electrode. This causes the two primary electrodes to break down, thus allowing current to flow across the gap. This process sends a voltage pulse to the center pin of switch #2, which again causes an arc between the center pin
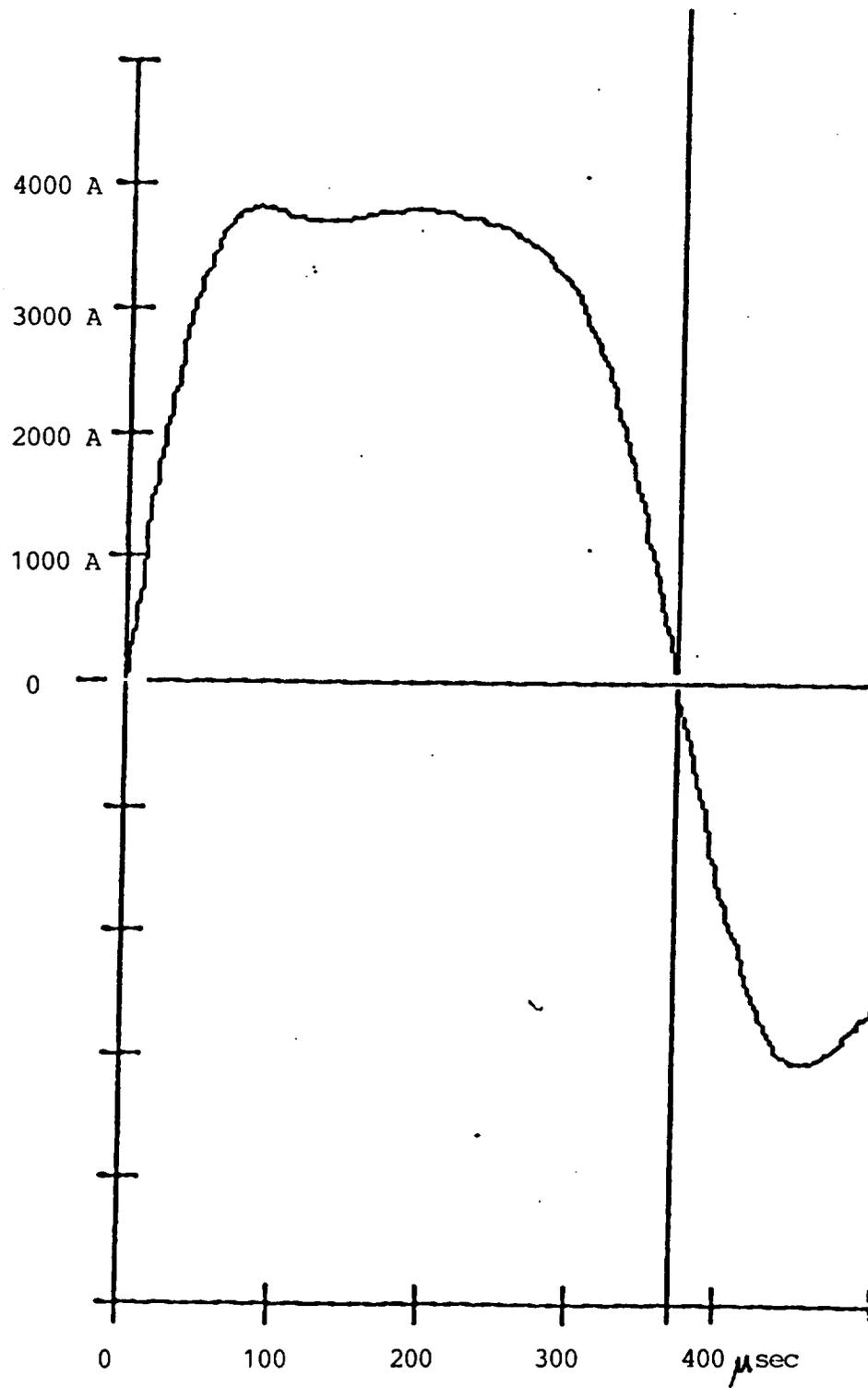
Figure 23. PFN Circuit Current With 12 kV Charge,

$L_1=L_2=L_3=L_4=$ 100 μH, $\quad$ $C_1=C_2=C_3=C_4=$ 14 μF, $\quad$ $R_M=$ 0.5Ω
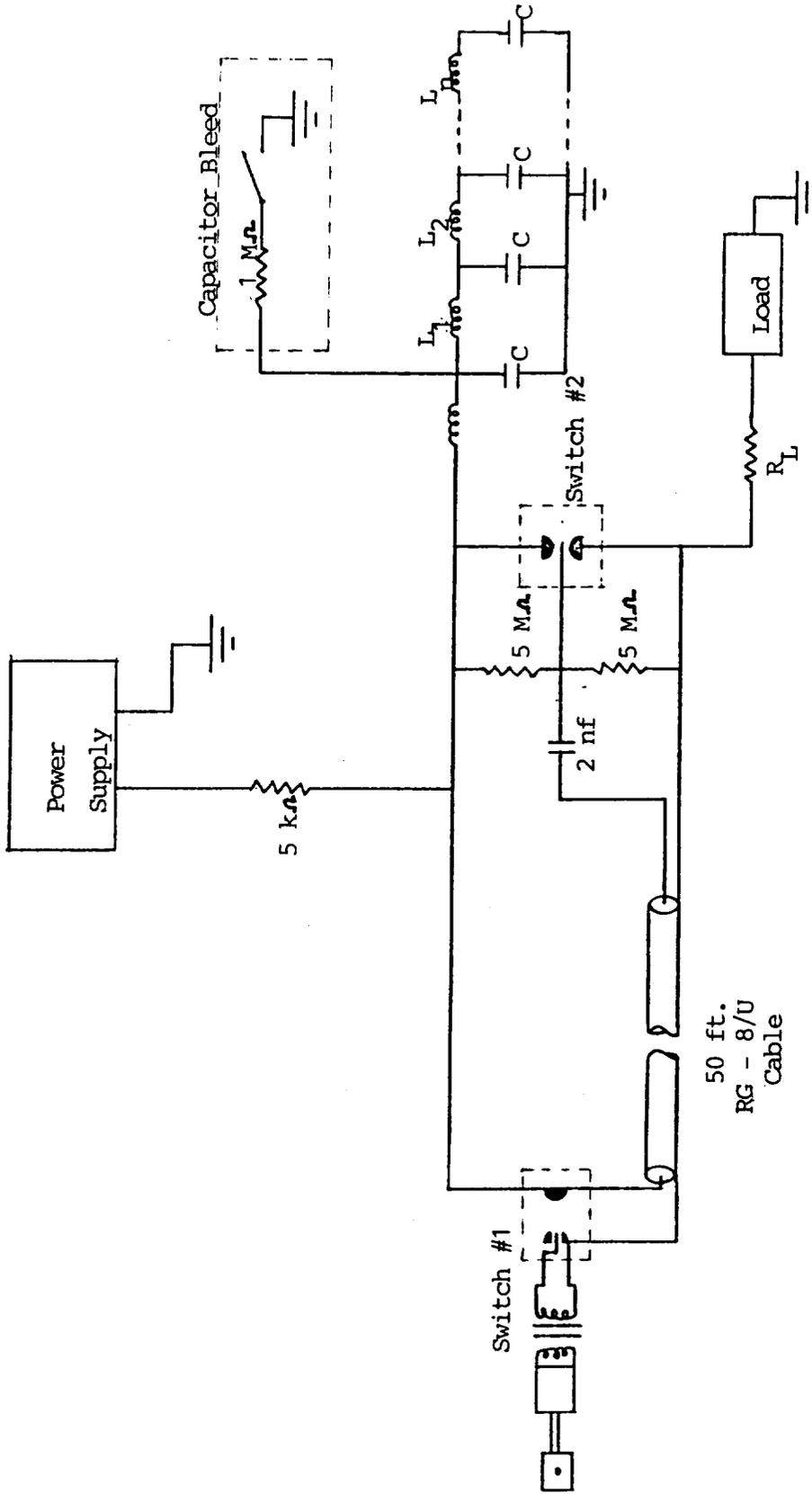
Figure 24. Circuit Diagram of Electrical Discharge System

and electrode. This, in turn, causes a breakdown which allows the capacitor bank current flow to the load. One purpose of using two switches is to isolate the controller from the high currents.

4. Electrical Discharge Devices: Plasma Source

The primary device to be used in this study is the ablative thruster. It consists of an aluminum anode, a brass cathode, and a block of polyethylene fuel positioned between the anode and cathode. Figure 25 illustrates this. Plexiglass is used to insulate the cathode from the anode. This forces the arc to be driven from the anode through the polyethylene to the tip of the cathode. The arc ablates the polyethylene which is then exhausted through the hole. The ablative process allows plasma to be formed while avoiding the build up of back pressure due to the initial unsteady flow created by the gas feed system. This allows the experiment to be operated for sufficient run times at the desired back pressures.

A coaxial thruster has been used for the initial testing of the electrical discharge and vacuum systems. The thruster consists of an aluminum anode and cathode, as shown in Figure 26. This thruster is fired by bleeding nitrogen into the evacuated system and allowing the gas to fill the space between the anode and cathode. This thruster has been fired consistently allowing the initial testing and development of the experiment to proceed smoothly.

The magnetic field coil will be used to study the acceleration of plasma exhausted from the ablative thruster. It is made by coiling 0.25-inch diameter, solid copper wire around an 8.75-inch outer diameter, schedule 40 PVC pipe. Specifically, there are two layers of five wraps of wire. With this configuration, a magnetic field of 1.5kG can be produced at the center of the coil with a current of 3kA.

5. Diagnostics of the Experimental Set-Up

Two basic diagnostics have been used to determine the output of the electrical discharge system. The first is a Rogowski loop which is used to measure the current wave form of the PFN. The output of the loop is fed through a passive integrator to a Tektronix Type 551 Dual Beam Oscilloscope (Beaverton, Oregon). The output is recorded by a Tektronix C-27 Oscilloscope camera using

ABLATIVE
MATERIAL

ABLATIVE MATERIAL

1 cm

ANODE

CATHODE

Aluminum

Plexyglass

Brass

Polyethylene

O-Ring
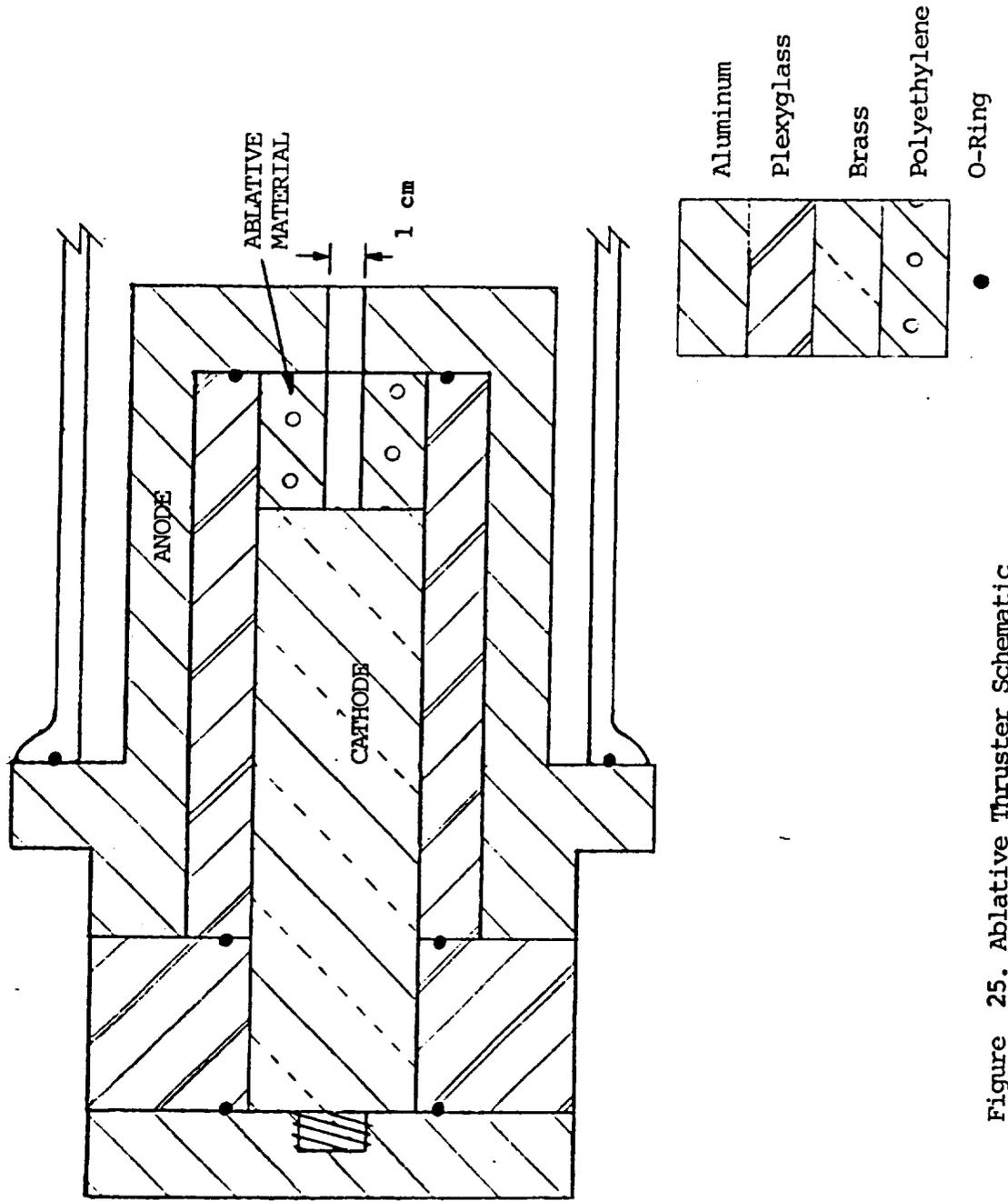
Figure 25. Ablative Thruster Schematic
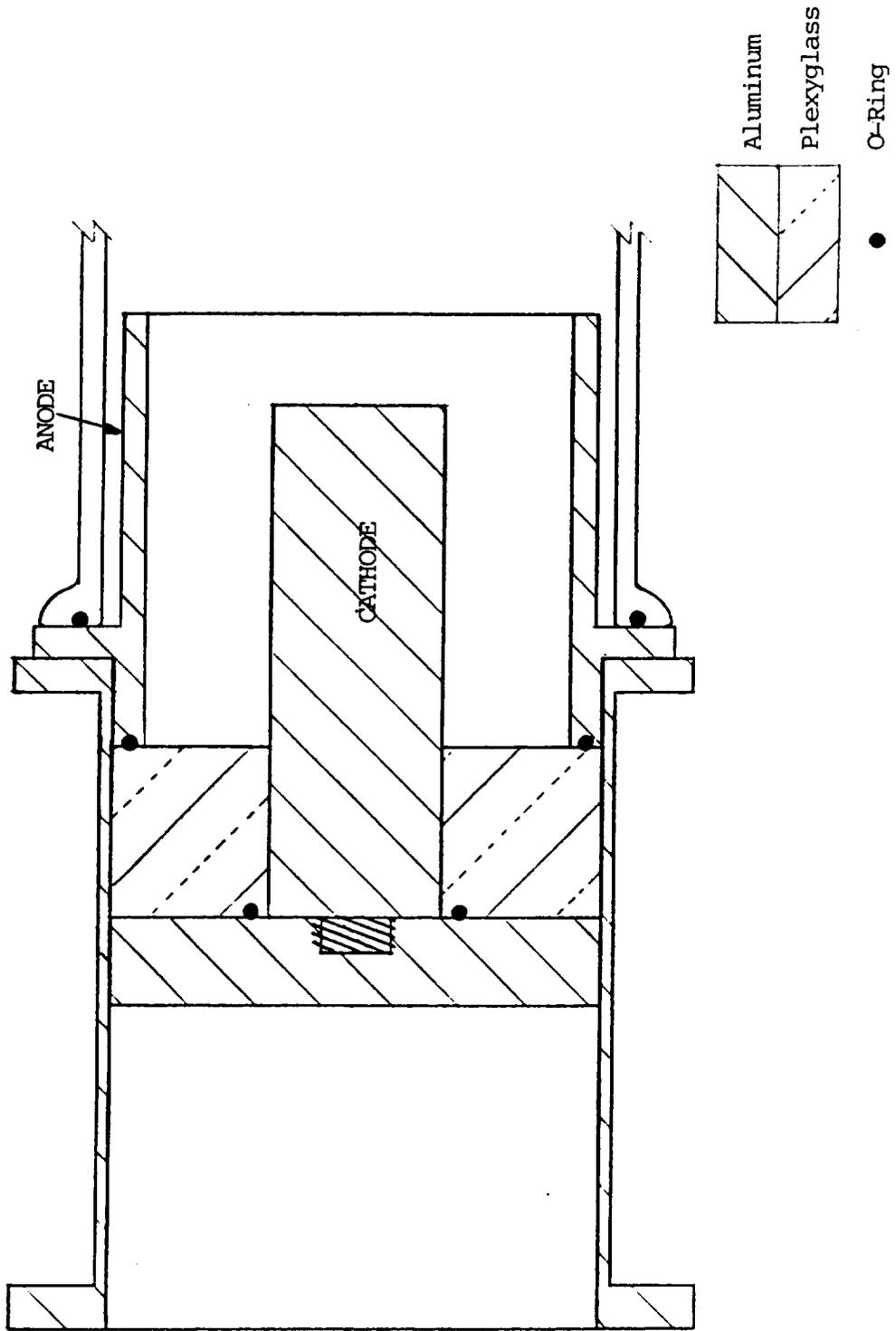
Figure 26. Coaxial Thruster Schematic

3,000 ASA film. The Rogowski loop was calibrated by measuring the known response of a simple L-C circuit. Examples of typical output are shown in Figure 28.

A second diagnostic used is a local magnetic field probe which measures the axial field of the magnetic field nozzle. This probe is a multi-coiled wire with a diameter of 3mm. The output of this probe is sent through a passive integrator to an oscilloscope and recorded. Examples of typical output are also shown in Figure 28.
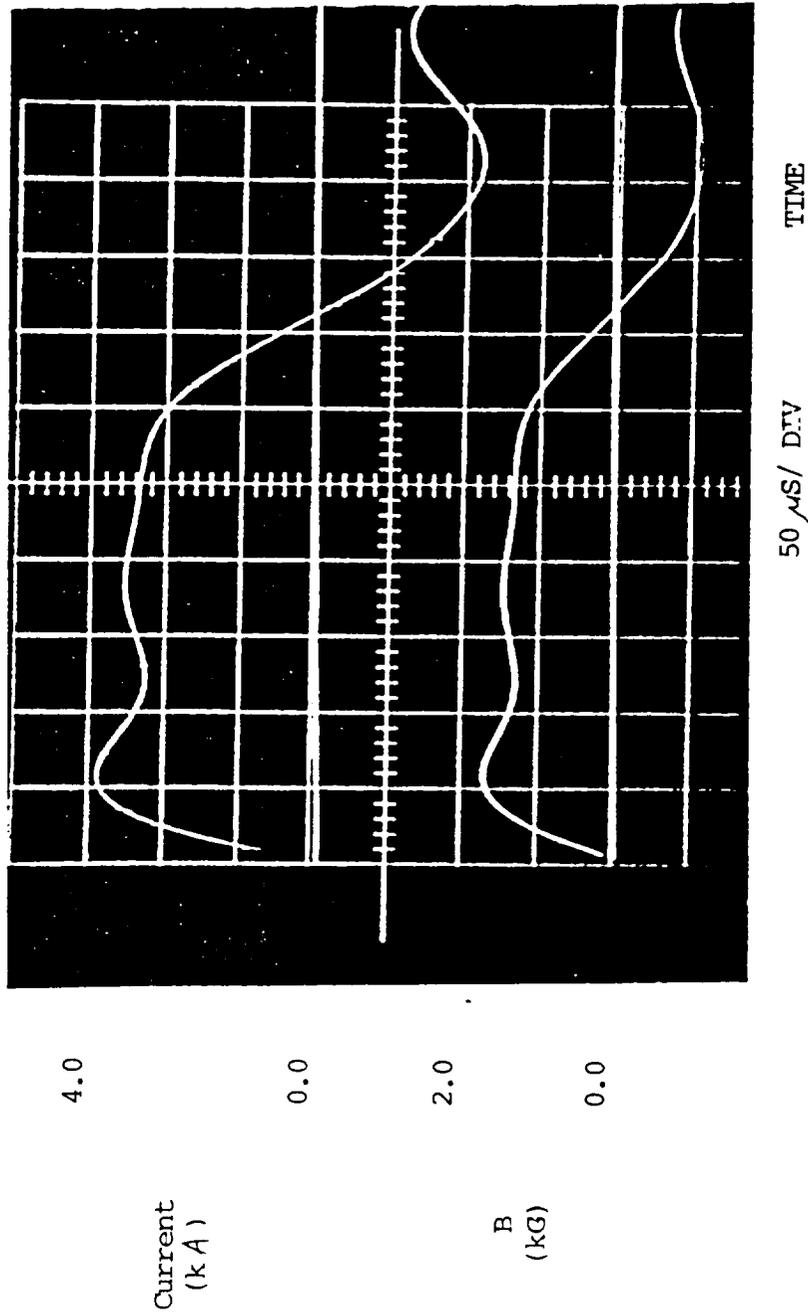
Figure 28. Measurements of Circuit Current and Magnetic
Field On-Axis in the Magnetic Nozzle. (12KU Bank Charge)

IV. EXPERIMENTAL STUDY OF A 1/4-SCALE MAGNETOPLASMADYNAMIC MPD THRUSTER
(Zakrzwski)

1. Introduction

The MPD thruster is a deice that operates with currents on the order of 5-15kA; related power requirements are on the order of megawatts. Since such power levels will not soon be available in space, there is interest in studying devices which can operate at power levels of 10-30kW. One such device is the 1/4-scale MPD.

The primary purpose of this study is to test a 1/4-linearly-scaled MPD thruster to determine the scaling characteristics of the electromagnetic component of thrust. This study would aid in the understanding of how an MPD thruster can be optimally sized and coupled to an optimum size power supply for a particular mission. Previous studies[7,8] have shown that smaller thrusters are more efficient than larger full-scale "benchmark" thrusters for certain power supply limitations and specific impulse ranges. In using a 1/4-scale device, this study will complement previous scaling studies, which utilized a 1/2-scale MPD, and will focus specifically on the electromagnetic thrust component which is the thrust component that offers the greatest possibility in improved efficiency. The 1/4-scale thruster will be operated both with and without applied magnetic nozzles. This will allow the study of the effectiveness of using a magnetic nozzle to recover frozen flow losses.

Work on this study was initiated at the Air Force Astronautics Laboratory (AFAL) at Edwards Air Force Base California, as part of a Co-Op arrangement between the Air Force and The Ohio State University. This work is presently being continued at Ohio State. Work done at AFAL was focused in three major areas. The first area was the design and construction of the 1/4-scale thruster which was based on the design of AFAL's 1/2-scale "benchmark" thruster. The second area of work was the testing of the 1/4-scale thruster using two different power supplies. The third area of work was the construction and testing of diagnostic equipment on the thruster. Current work at Ohio State is focused on the design and testing of a gas-pulse system to feed propellant through the thruster. A gas-pulse system different from that used at AFAL is needed because of the limited size of the vacuum chamber at Ohio State.

2. Design of the 1/4-Scale Thruster

The thruster for this study was designed so that all of the major linear measurements are half the value of these measurements on the AFAL's own 1/2-scale "benchmark" thruster. This was done so that a direct comparison between the two thrusters operating at AFAL could be made. A schematic of the thruster is given in Figure 29. This thruster was constructed with a copper anode having an inner diameter of 2.5 cm and an outer diameter of 4.5 cm. The cathode is made out of 2% thoriated tungsten and has a diameter of 0.5 cm. both the anode and cathode have a length of 1.25 cm as measured from the boron nitride backplate. Gas is fed into the discharge chamber through eight 0.3 mm diameter holes that are evenly spaced around the cathode midway between the anode and cathode radii. The thruster is mounted on a plexiglass stand. Both the anode and cathode are separated from the plexiglass by boron nitride to prevent ablation of the plexiglass. To electrically isolate it, the outer circumference of the cathode was wrapped with fusion wrap.

The 1/4-scale thruster was designed to operate at conditions that would produce a theoretical electromagnetic thrust density equal to the electromagnetic thrust density produced in a full-sized "benchmark" thruster operating at typical condition. The electromagnetic thrust density, f_z, is given by

$$f_z = j_z B_\theta$$

where j_z is the radial current density and B_θ is the azimuthal magnetic field.[9] It can be shown that

$$f_z \propto \frac{I^2}{r^2 L}$$

where I is the total current, r is the inner cathode radius, and L is the length of the discharge chamber.[9] For a full-size thruster operating at current of 10kA with a mass flow rate of 1.0 g/sec., the 1/4-scale thruster needs to operate at current level of 1.25kA with a mass flow rate of 0.0625 g/sec. to be scaled properly. The mass flow rate is scaled to keep the gas densities in the discharge chamber a constant for varying sized thrusters. The length of the discharge chamber was chosen so that if the thruster was run at 200 A for 15μ sec., the energy needed to ionize all the gas in the discharge chamber would only

Nylon Bolt

.280" R

1.750" Dia

.984" Dia

.050" R

Plastic
Tube

Tygon Tubing

.250"

Side View

Boron Nitride

Copper

Plexyglass

Tungsten
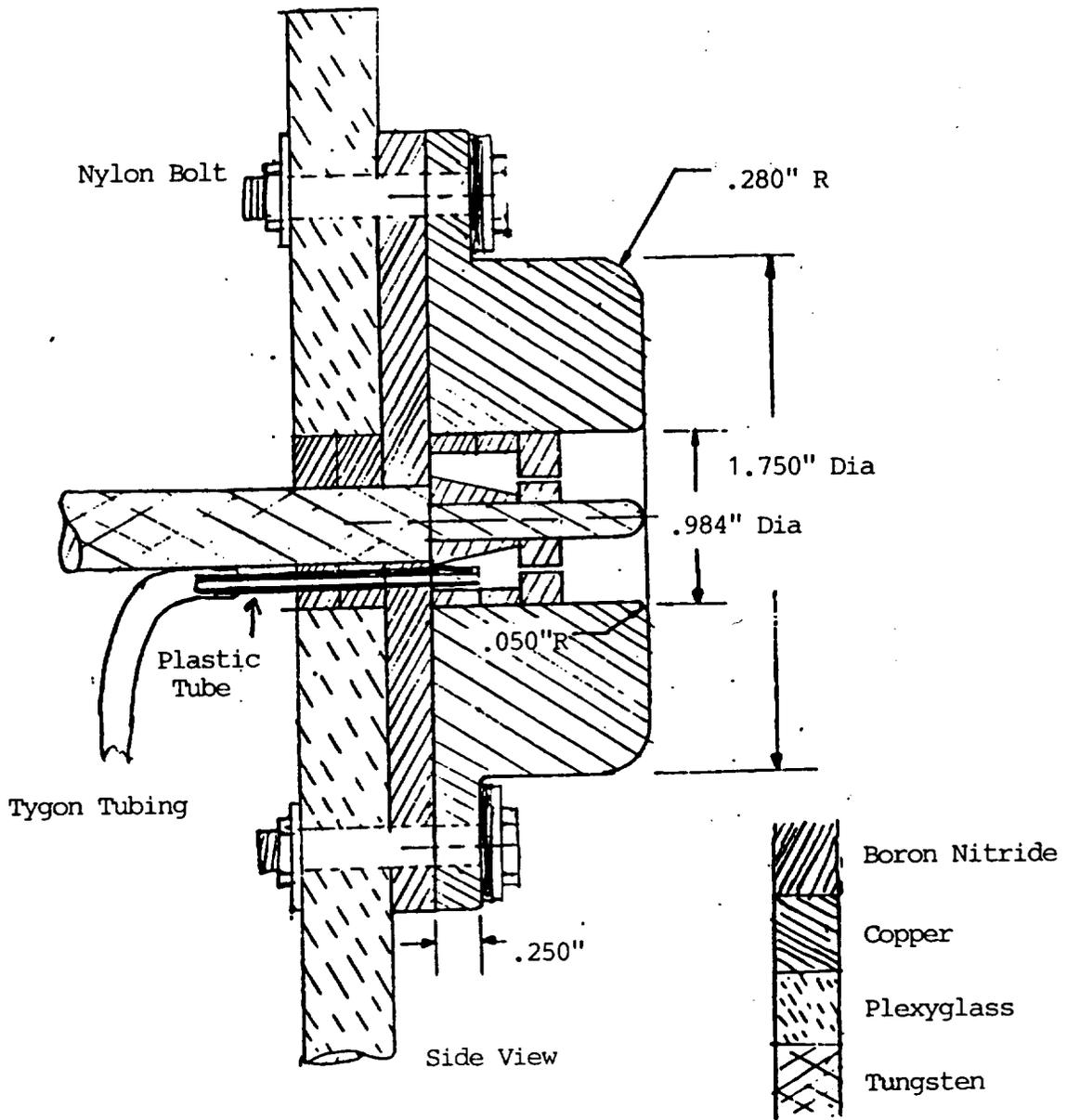
Figure 29. ¼-Scale MPD Thruster

be approximately 10% of the total available energy. This would allow for significant magnetic interaction to take place when the thruster was run off of the lower power preionization system at AFAL.

3. Test Firing of the 1/4-Scale Thruster at AFAL

The 1/4-scale thruster was fired at AFAL using two different power supply systems. For these tests the firing was taped on a VHS cassette. Measurements of the current and voltage characteristic were attempted during these tests. A significant range of the current-voltage relation could not be measured because of difficulties that arose in the existing facility and because of extraneous arcing in the thruster.

The 1/4-scale thruster was initially fired using a modified version of the preionization (PI) circuit at AFAL; that system was designed and fabricated by the Principle Investigator, T.M. York. The modified circuit is shown in Figure 30. The charge for this power supply is held in a 0.4μ F capacitor that was charged between 2kV and 3kV. To allow the thruster to operate at two distinct power levels, two interchangeable inductors were constructed to be put in series with capacitor. A 55μ F inductor gave an initial pulse length of 15μ sec. with a maximum amplitude of 220A. A 225μ F inductor gave an initial pulse length of 30μ sec. with a maximum amplitude of 110A. The range of voltages on the capacitor that allowed the thruster to discharge consistently was small. The thruster would fire at 2,300 V $\pm$ 25 V when the 55μ F inductor was used and at 2,100 V $\pm$25V when the 225μ F inductor was used.

Attempts were made to operate the 1/4-scale thruster using the AFAL's Pulse Forming Network (PFN). This network had a total capacitance of $60,000\mu$ F and could be charged up to 800 Volts. The move to use the PFN was caused by AFAL's need to test the PFN and the desire to operate the 1/4-scale thruster at higher power levels. The 1/4-scale thruster failed to fire consistently using the PFN as the power source. This failure is thought to be due to the bank design and the need of the PFN to operate with a preionization system. Several methods to preionize the flow, such as discharging ionized gas from a miniature electrode configuration into the 1/4-scale thruster, did not prove successful. The original preionization system was not used as it was designed to be because of the length of time it would take to correctly implement this system. After it
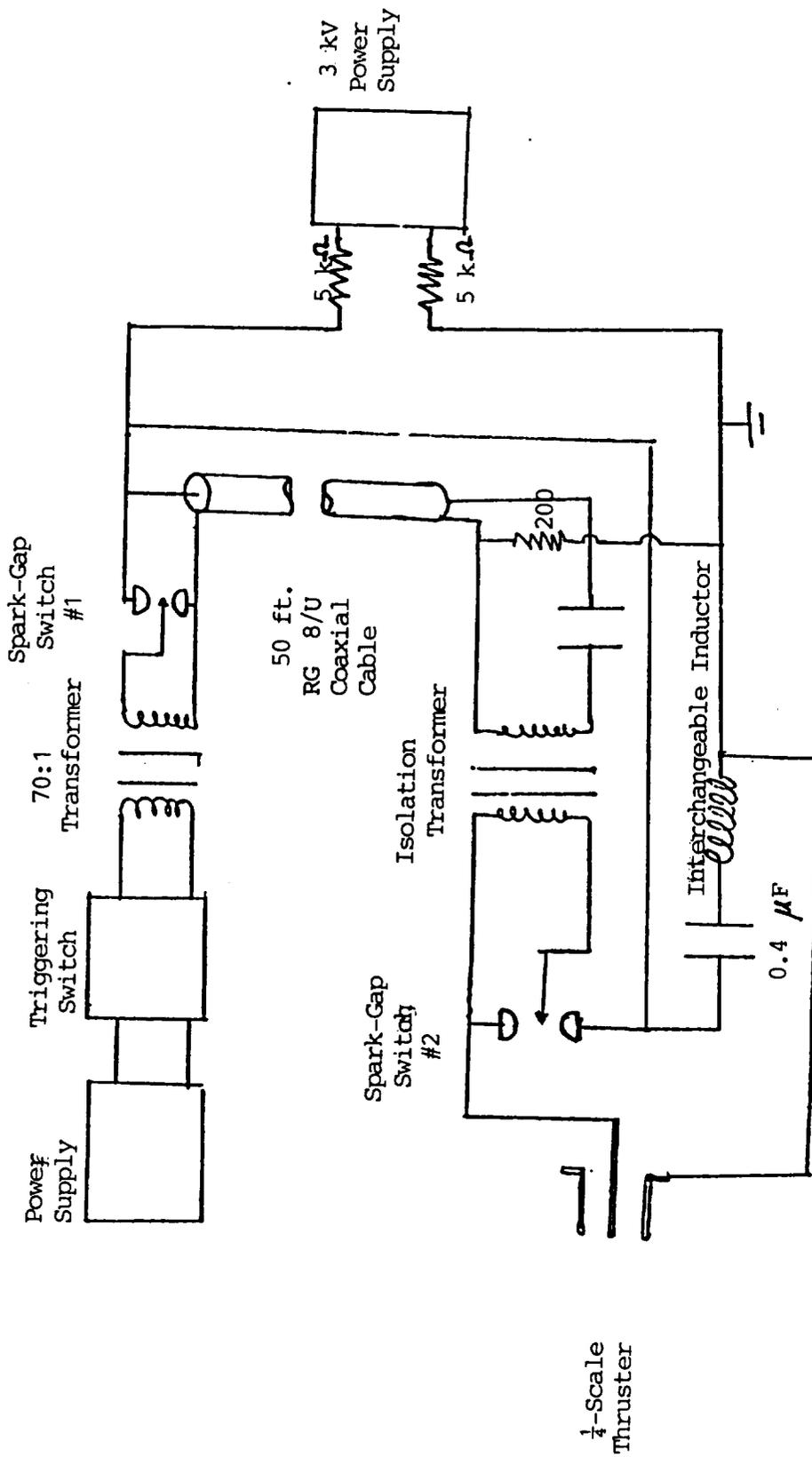
Figure 30. Modified Pre-ionization Circuit

was determined that the 1/4-scale thruster could not be tested with the PFN, the 1/4-scale thruster was reconnected to the modified PI circuit.

4. Diagnostic Work on the 1/4-Scale Thruster

To measure the performance of the 1/4-scale thruster, several types of diagnostic equipment were assembled. Initial measurements of the I-V characteristic of the thruster were made with a current probe (Pearson Model 401X) and a high voltage probe (Textronix Model P6015). While qualitative measurements were recorded with a four channel digital oscilloscope (TEAM System 8612), quantitative measurements could not be made until a faster sample two-channel oscilloscope (Nicolet 2090) was obtained. A typical measurement showed a 10 Volts for 220A while the thruster was operating at a mass flow rate of 1.0 g/sec. These measurements were made after the 1/4-scale was connected to the PI circuit the second time. A significant range of I-V measurements was not taken because the thruster began to misfire. The misfiring was discovered to be the result of arcing behind the backplate of the thruster. The problem was corrected by modifying the way the boron nitride pieces are fitted together. Tests run after the redesign show no arcing problems.

A magnetic probe and pressure probe were acquired for diagnostic work. A magnetic probe consisting of a 40 wrap multilayer coil sealed in a 0.8 cm diameter glass tube was constructed and calibrated. The probe responded well when tested with the thruster. Accurate data could not be taken at AFAL because of the above-mentioned difficulties. An existing piezoelectric pressure probe was modified so that the pressure in the thruster exhaust plume could be mapped. This probe consists of a pressure transducer (PCB 113A21) fixed to the inside end of a quartz tube. The probe is electrically insulated with metal foil wrapped around the inner circumference of the tube. A quartz cap is fused on the outside front of the tube and has an insulating metal cap fastened over it with insulating tape.

Diagnostic measurements of the 1/4-scale thruster at Ohio State will be made with the above-mentioned magnetic and pressure probes. The I-V characteristic of the thruster will be made with existing equipment at Ohio State. The plume diagnostics will be done both with and without the magnetic nozzle.

5. New Development Gas-Pulse System for 1/4-Scale Thruster

A new gas-pulse system to feed propellant to the 1/4-scale thruster has been designed. This new system is needed because the vacuum chamber at Ohio State is much smaller that chamber at AFAL. The new gas valve opens very fast (microseconds) so that a steady gas flow through the thruster can be established without flooding the vacuum system with gas and raising the back pressure above desired limits.

The "fast" gas valve is based on the valve originally designed by Fisher.[10] A diagram of the valve itself can be seen in Figure 31. The valve opens when a large current is sent through the solenoid by discharging the capacitors. The solenoid produces a magnetic field which sets up eddy currents in the aluminum hammer. The eddy currents interact with the magnetic field and produce a JxB force which lifts the hammer upward. Once the hammer is lifted the test gas can flow from the reservoir to the thruster. Compressed air acts on the top of the hammer to keep the valve closed prior to opening. By using a total capacitance of 30μ F charged to 30kV, the time for the gas to reach a steady flow is expected to be close to the 20μ sec. response Fisher obtained with his valve.[11] The "fast" valve will allow the 1/4-scale thruster to operate for $100-200\mu$ sec. while keeping the background pressure of the order of 10^{-5} torr.

Pattern	Label
Value Casing	Value Casing
Aluminum Hammer	Aluminum Hammer
Solenoid	Solenoid
Compressed Air	Compressed Air
Working Gas	Working Gas
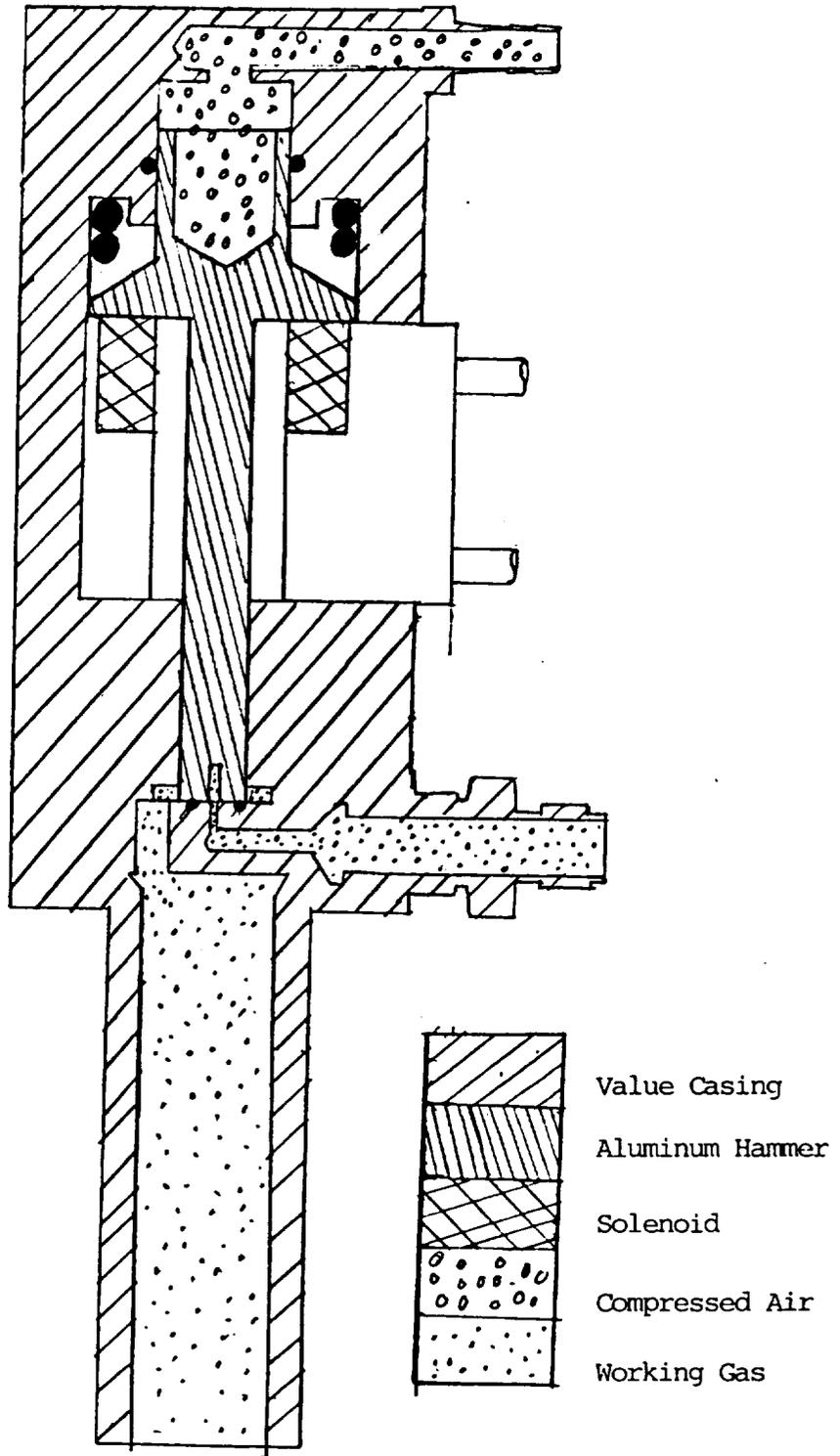
Figure 31. Fast Gas Value Schematic

V.   THOMSON SCATTERING DIAGNOSTICS FOR PLASMA FLOW IN A MAGNETIC NOZZLE
GEOMETRY

1.   Introduction

Diagnostic techniques that are both non-intrusive and accurate in determining local conditions are quite important in plasma studies. Thomson scattering, while difficult and expensive to implement, has proven to be a reliable indicator of plasma properties.[12,13] In the studies to be carried out as part of this project, there is the added complication of strong magnetic fields at locations where diagnosis is of interest. Such effects do not interfere with the ability of TS to indicate electron density (N_c) and electron temperature (T_e) with absolute certainty.

2.   Application of the Thomson Scattering Diagnostic

There are four constraints that must be observed in order for the Thomson scattering diagnostic to work. First, operation must occur in the incoherent region of scattering. Second, the detection system should properly resolve the details of the frequency spectrum. Third, the laser beam path should be constructed to avoid false scattering from the beam itself (so-called stray light). Finally, fourth, sources of extraneous signals (noise) due to the plasma and to the photon-counting statistics should be evaluated to determine that they do not overwhelm the scattered signal from the plasma.

In order for the scattering to be in the incoherent regime,

$$1/k_d \lambda_D < 1 \quad . \tag{1}$$

Here λ_D is the Debye length. Using the definition of λ_D and Equation (1), this condition becomes $\dfrac{1.08 \times 10^{-4} \lambda_i \text{ (cm)}}{\sin \theta_s/2} [\dfrac{n_e}{T_e \text{(eV)}}]^{1/2} < 1 \quad .$

For a ruby laser with an angle of θ_s of 90 degrees, this reduces to

$$n_e/T_e < 10^{15} \text{ cm}^{-3} - \text{eV}^{-1} \quad . \tag{2}$$

This criterion was satisfied by the plasma generated by the 50-cm long theta-pinch experiment.

The temperature can be derived from the scattered-wavelength spectrum through a determination of the $1/e$ half width of that spectrum; the $1/e$ half width is given by the difference between the center wavelength of 6943 A and the

wavelength where the scattered signal is down by a factor of $1/e$ from that at the center of the spectrum at 6943 A. The $1/e$ half width is given by

$$\Delta\lambda_{1/e} = (2a\lambda_i \sin\frac{\theta_s}{2})/c \quad ,$$

which for a ruby laser with $\theta_s = 90$ degrees gives

$$\Delta\lambda_{1/e} = 19.7T_e^{1/2}(eV)(\overset{\circ}{A}) \quad . \tag{3}$$

Accordingly, resolution of the temperature means resolution of the $1/e$ points of the scattered-wavelength spectrum.

Since the scattered laser signal is small (a factor of 10^{-16} of the incident beam intensity) any stray light from the main beam itself can overwhelm the scattered signal. Significant stray light sources occur where the laser beam encounters the entrance and exit windows of the plasma device. The material used for these windows should be as free from internal imperfections as is reasonably possible. They must also be kept scrupulously clean to avoid dust which can act as a major scattering source for the incident beam. Nevertheless, there will still be stray light from these windows, and apertures are needed inside the discharge tube to reduce the problem. At the exit window the beam should be absorbed so that it is not reflected back through they system. This can be done with an absorbing blue glass beam dump (Corning CS-74 blue glass) set at the Brewster angle to minimize reflection at the exit window. Again, a series of apertures just before the beam encounters the exit window is useful in minimizing returning reflections. Also, if a black, absorbing background is viewed by the detection optics, it aids again in reducing stray light that may bounce off the wall of the discharge tube and they enter the collection space of these optics. In actual practice, it is necessary to completely cover the pinch with black cloth to make it "light tight" against laser light reflected and scattered outside the vacuum vessel.

The two sources of noise are the plasma breamsstrahlung and the Poisson statistical nature of the photon detection process. There are generation of the photoelectrons.[14] Thus, the signal to noise ratio is expressed as

$$\frac{S}{N} = N_{pe}^{1/2} = \left\{ \frac{P_i r_{eo}^2 d\Omega n_e L\eta_d}{ha(2\pi)^{1/2}} [\hat{s} \times (\hat{s} \times \hat{E}_{lo})]^2 \exp[-c^2\Delta\lambda^2/(2a^2\lambda_i^2)]r_L d\lambda_s \right\}^{1/2} \tag{4}$$

3. <u>Thomson-Scattering Diagnostic Apparatus</u>

The Thomson-scattering apparatus to be used in the experiment is shown in Figure 32. Both the entrance and exit windows will be placed at the Brewster angle to minimize reflection and to maximize transmission of the main beam. The windows will consist of common place glass in the form of 1/4-inch thick, 7-inch diameter discs. Apertures will clean the beam of high-divergence light before it enters the vacuum vessel. They will also be needed after the entrance window to reduce stray light effects due to the window. The scattering will be done at a 90 degree angle. The laser source was an Apollo model 35 ruby laser which used an oscillator and a one-pass amplifier arrangement. This laser was manufactured by Apollo Lasers, Incorporated, of Los Angeles, California. It provides 7J into a 3-mrad divergence cone with a 3/4-inch diameter beam for a 25-nsec pulse. Three components of this diagnostic system will now be noted: the focusing optics, the detection optics, and the detectors.

The focusing optical train consists of beam-cleaning apertures plus a converging lens system. The detection optics will consist of a converging lens, an aperture, converging lens, a beam splitter, and two wavelength filters. The beam will be split into two paths by the beam splitter and subsequently be detected by the photomultipliers. The filters have a 30-A full bandwidth at half maximum and perform the function of separating the wavelength spectrum into two components for temperature determination. One filter will be set at normal incidence to the light and its wavelength passband centered on 6943 A. This fixes the peak point of the scattered-wavelength spectrum. The other filter will be set at an angle α_f to normal incidence. This has the effect of tuning the filter according to the equation

Here $\lambda(0°)$ is the peak transmission wavelength for the case of normally incident light, $\lambda(\alpha_f)$ is the peak transmission wavelength for the angle α_f, and n_f is the index of refraction for the filter material.

The detectors to be used are two RCA 7265 photomultipliers purchased from the Electro Optics Division of RCA located in Lancaster, Pennsylvania. These tubes have a peak bias voltage of -3 kV where maximum amplification from the photon multiplication process occurred. No other amplification will be necessary

Figure 32 Schematic of Thomson Scattering Diagnostic System

and the output of the tubes will be input to an oscilloscope with a 50-Ω resistor acting as the cable-terminating load.

   To monitor reproducibility in the laser beam energy, a photodiode beam monitor, as shown in the beam input optical train will be used. The diode samples the beam and provides a measure of the energy in the laser beam. This signal will then be used to normalize the laser-scattering data taken. The main laser beam will be sampled by a piece of plate glass placed at an angle to the beam. This glass piece acted to divert four percent of the beam to the photodiode. The photodiode signal will be calibrated using a calibrated laser calorimeter to measure the beam energy after the plate glass reflector.

VI. PROPOSED NEW DIAGNOSTIC STUDIES

1. Introduction

The work being carried out on this project is coupled to related studies being supported by AFOSR. Specifically, the development of new diagnostics to move clearly understand mechanisms and transport processes active in plasma thrusters is being supported. The hint of the diagnostics being studied is a CO_2 laser system. Its procurement will be initiated during the next six months. A proposal to initiate new diagnostic studies is presently under consideration and some details of that proposal will be repeated below.

2. Plasma Properties in the Thruster Exhaust Field

The plasma being ejected from MPD type device has been categorized by a number of research studies. In 1971, NASA-Lewis reported Thomson scattering measurements in the exhaust of a nitrogen MPD: at 20kA, and 11.2kA 30 cm from the exit plane Ne $\approx$ $8x10^{13}$ cm^{-3}, Te $\approx$ 5 eV. With argon, a propellent, a spatial variation of properties was reported by E.M. Campell (Princeton EPL) in 1977, who used Langmuir probes: at 4kA with 12g/Sec, Ne - $6x10^{14}$ cm^{-3} to 2 x 10^{13} cm^{-3} between 0 and 30 cm on axis while Te - 12,000°K to 4,000°K between 0 and 30 cm. In 1985, an MPD operated at AFAL was diagnosed with Langmuir probes developed by the principal investigator and indicated Te $\approx$ 2eV at 25 cm, while Ne - 4.48 x 10^{15} at 20 cm and Ne - 1.9 x 10^{15} at 30 cm.

Based on the above evaluations, it is anticipated that source plasma generated by 4kA will produce plasmas with Ne $\approx$ 10^{15} cm^{-3}, 4eV and will expand to Ne $\approx$ 10^{14} cm^{-3}, Te $\approx$ 2eV at 30 cm. These are critical values when designing a diagnostic system.

3. Proposed Research Studies

The effort to be carried out will involve three different diagnostic measurements with the CO_2 laser based system: (1) multi-beam interferometry; (2) Faraday-rotation measurements of local B-field; and (3) fluctuation studies. Each of these has its own inherent difficulty; i.e., this is not an application of off-the-shelf type techniques, but the application of recently reported, physically proven techniques which will require careful experimental design and unique components to produce useful results. Generally, the list above is

indicative of increasing difficulty. A one year effort, especially with a significant percentage being carried by a (new) graduate student researcher, must concentrate on the simpler techniques in order to optimize results. Accordingly, some techniques (2 and 3) will receive careful and complete evaluation with respect to experimental design, while emphasis will be directed to accomplishing measurements with the multi-beam interferometer.

3.1 Multi-beam Interferometer

This technique generally utilizes a Mach-Zender configuration. A measurement of phase shift (ϕ) allows determination of electron density as

$$\phi = 2.82 \times 10^{-13} \, \lambda_o \int_{Z1}^{Z2} Ne(Z)dZ \qquad \text{(cgs units)}$$

When λ_o is the laser wavelength, Z is the path variable through the plasma. In the above, measurement of ϕ indicates the integrated line density.

Clearly, one can see the importance of CO_2 radiation at $10\mu m$ as compared to say, red light at 6973Å. Also, the unfolding of an axisymmetric profile of Ne requires a large number (2-5) of interferometer channels. Successful applications of this technique with CO_2 lasers have produced time histories of profiles of Ne(r) over a period of 20 ms with Ne $\approx 10^{15}$ cm^{-3} and 1 $\approx$ 10 cm. Considerable care will have to be exercised in detector selection to be successful. The use of a Bragg cell to modulate the beam has proven successful and that technique will be pursued. Care will have to be taken with the beam deflection (α) due to gradients, as $\alpha \sim M_o \, \lambda_o^2$, and this could cause problems in location of detector windows. Another advantage of large λ_o is that the sensitivity to mechanical vibration decreases; specifically, when $\lambda_o > 4 \times 10^8$ [$\Delta e/r_o n_o$] where Δe is vibration induced path change and r_o is plasma radius.

3.2 Faraday Rotation Measurements of B field - Polarimetry

The determination of local, unperturbed magnetic field is quite difficult; all experimenters use physical loops placed in the plasma. This disturbs the signal, cools the plasma, and alters current conduction path. So, a nonintrusive technique is quite valuable. Through Maxwells' equation, the local current density can also be determined.

The basic principle of this measurement is that the plane of polarization of a laser beam will be rotated proportional to B, as

$$\theta \text{ (deg)} = 1.5 \times 10^{-12} \lambda_o^2 \int_0^1 NeB_{11}(kG)dl$$

Clearly, a large λ_o will allow significant θ to be generated even though B_{11} (the component of B along propagation) will be small. Specifically with Ne $\simeq$ 10^{15} cm^{-3} and $1 \simeq 10$ cm, the θ with CO_2 radiation would be very difficult to measure. However, using 118.8 μm will produce a rotation of greater than 1 degree. It can be seen that the signal involves the product, Ne B_{11}, so the results from the CO_2 measurement of Ne(r) will be critical to accurate determination of $B_{11}(r)$ profiles.

3.3 Measurement of Electron Density Fluctuations

This technique is based upon the principles of Thomson scattering - scattering from free elections and ions. The ability to measure fluctuations, which are extremely important because they generate anomalous transport, is related to a number of factors. The characteristic parameter for Thomson Scattering is $\alpha = 1/k\lambda_D = \lambda_o/4\pi\lambda_D \sin(\theta_s/2)$ where λ_D is the Debye length and θ_s is the scattering angle. The range, $\alpha \ll 1$, defines normal Thomson Scattering for

Te, Ne. When $\alpha \gg 1$ plasma waves and thermal ion fluctuations may be studied
and ion temperature determined.

Wave scattering can result in large enhancements in the scattered power,
well above those achieved with thermal motion, as scattered power is

$$Ps = \frac{1}{2} P_o r_e^2 \ \lambda_o^2 (\tilde{N})^2 Lv$$

Where P_o is incident power, r_e is electron radius, λ_o is incident wavelength, $\tilde{N}$
is defined by $\tilde{N}$ core $(kZ-wt)$ and Lv is the length of the scattering volume. CO_2
lasers with 10-100 W can be used, but also, FIR lasers generating 119 μm at 10-
100 mW output power levels have been sufficient to perform scattering measure-
ments with good signal-to-noise ratios. One critical element in the type of
measurement is a low-noise fundamental mode mixer. Fluctuation measurements
over a range of frequencies have been made with plasmas similar to those expected
in MPD exhaust flows.

VII. FACULTY AND STAFF PARTICIPATION

T.M. York	Principle Investigator Jan. 1, 1988 - Dec. 31, 1988	10%
D.S. Emmer	Research Associate Sept. 1, 1988 - Dec. 31, 1988	10%
P. Mikellides	Graduate Research Associate June 15 - Aug. 30, 1988 Sept. 1 - Dec. 31, 1988	50% 25%
G. Soulas	Graduate Research Associate June 15 - Dec. 31 1988	50%
C. Zakrzwski	Graduate Research Associate Sept. 1 - Dec. 31, 1988	25%
J. Smolka	Undergraduate Assistant June 15 - Aug. 30, 1988 Sept. 1 - Dec. 31, 1988	50% 10%

VIII. REFERENCES

1. Jacoby, B.A., "Experimental investigation of energy loss and end loss physics in a linear theta pinch", (Ph.D. Thesis, Penn State University) DOE Report ET-53018-4, January, 1981.

2. Stover, E.K., "Computer simulation of plasma behavior in open-ended linear theta machines" (Ph.D. Thesis, Penn State University) DOE Report ET-53018-6, April, 1981.

3. Braginskii, S.I., "Transport Processes in a Plasma," in Reviews of Plasma Physics, edited by M.A. Leontovich, 1, 217, Consultants Bureau of New York, 1965.

4. Spitzer, L., Jr., Physics of Fully Ionized Gases, Wiley, New York, 1956.

5. Woods, L.C., Principles of Magnetoplasma Dynamics, Oxford Science Publications, New York, 1987.

6. Lorrain, P. and Colson, D.R., Electromagnetic Fields and Waves, 2nd edition, W.H. Freeman and Company, New York, 1970.

7. Mead, F.B. and Jahn, R.G., "Scaling of MPD Thrusters," AIAA Paper 79-2075, AIAA 14th International Electric Propulsion Conference, Princeton, New Jersey, October 30-November 1, 1979.

8. Kaplan, David I. and Jahn, R.G., "Performance Characteristics of Geometrically-Scaled Magnetoplasmadynamic (MPD) Thrusters," M.S.E. Thesis, MAE Report 1492, Princeton University, Princeton, New Jersey, February 1982.

9. Jahn, R.G., Physics of Electric Propulsion, McGraw-Hill Book Company, New York 1968.

10. Fisher, A., Mako, R. and Shiloh, J., Rev. Sci. Instrum., pp.832 (1978).

11. Shiloh, J., Fisher, A., and Rostoker, N., American Physical Society, Vol. 40, No. 8, February 20, 1978.

12. Sheffield, J., Plasma Scattering of Electromagnetic Radiation, Academic Press, New York, 1975, p. 115.

13. Kunze, H. J., "The Laser as a Tool for Plasma Diagnostics," Plasma Diagnostics, ed. by W. Lochte-Holtgreven, North Holland Publishing Co., Amsterdam, 1968, p. 584.

14. Sheffield, J., Plasma Scattering of Electromagnetic Radiation, Academic Press, New York, 1975, p. 67.